Journal of Zhejiang University-SCIENCE B (Biomedicine & Biotechnology) in press
www.jzus.zju.edu.cn; www.springer.com/journal/11585
E-mail: jzus_b@zju.edu.cn

Research Article

https://doi.org/10.1631/jzus.B2500154

Alamandine inhibits pathological retinal neovascularization by targeting MrgD-mediated HIF-1α/VEGFA pathway

Kun Zhao[1,#], Yaping Jiang[2,#], Wen Huang[1], Yukang Mao[1,3], Yihui Chen[2], Peng Li[1]✉, Chuanxi Yang[4]✉

[1]*Department of Cardiology, The First Affiliated Hospital of Nanjing Medical University, Nanjing 210029, Jiangsu, China*
[2]*Department of Ophthalmology, Yangpu Hospital, Tongji University School of Medicine, Yangpu 200082, Shanghai, China*
[3]*Department of Cardiology, the Affiliated Suzhou Hospital of Nanjing Medical University, Suzhou Municipal Hospital, Suzhou 215000, Jiangsu, China*
[4]*Department of Cardiology, Yangpu Hospital, Tongji University School of Medicine, Yangpu 200082, Shanghai, China*

Abstract: Retinopathy of prematurity (ROP) is a vision-threatening disorder that leads to pathological growth of the retinal vasculature due to hypoxia. Here, we investigated the potential effects of Alamandine, a novel heptapeptide in the renin-angiotensin system, on hypoxia-induced retinal neovascularization and its underlying mechanisms. In vivo, the C57BL/6J mice with oxygen-induced retinopathy (OIR) were injected intravitreally with Alamandine (1.0 μM/kg per eye). In vitro, human retinal microvascular endothelial cells (HRMECs) were utilized to investigate the effects of Alamandine (10 μg/ml) on proliferation, apoptosis, migration, and tubular formation under vascular endothelial growth factor (VEGF) stimulation. Single-cell RNA sequencing (scRNA-seq) matrix data from GEO database and renin-angiotensin system (RAS)-related gene from the Molecular Signatures Database was sourced for subsequent analyses. By integrating scRNA-seq data across multiple species, we identified that RAS-associated endothelial cells populations were highly related to retinal neovascularization. The LC-MS/MS analysis revealed a significant decrease in Alamandine levels in both the serum and retina of OIR mice when compared to the control group. Next, Alamandine ameliorated hypoxia-induced retinal pathological neovascularization and physiologic revascularization in OIR mice. In vitro, Alamandine effectively mitigated VEGF-induced proliferation, scratch-wound healing, and tube formation of HRMECs primarily by inhibiting the HIF-1α/VEGF pathway. Further, coincubation with D-Pro^7 (Mas-related G protein-coupled receptor D (MrgD) antagonist) hindered the beneficial impacts of Alamandine on hypoxia-induced pathological angiogenesis both in vivo and in vitro. Our findings suggested that Alamandine could mitigate retinal neovascularization by targeting the MrgD-mediated HIF-1α/VEGFA pathway, providing a potential therapeutic agent for OIR prevention and treatment.

Key words: Alamandine; Pathological neovascularization; Retinopathy of prematurity (ROP); Oxygen-induced retinopathy (OIR); MrgD; VEGFA

Unedited

1 Introduction

Retinopathy of prematurity (ROP) is a vision-threatening disorder of multifactorial etiology that progresses to hypoxia-induced pathological growth of the retinal vasculature, resulting in permanent damage to the retina in preterm infants (Sabri et al, 2022). As a biphasic disease, ROP is initiated by oxygen therapy-induced delayed growth and degeneration of existing incomplete retinal blood vessels at birth, followed by the neovascularization of the retina and vitreous caused by the relatively hypoxic microvascular environment that cannot enable the adequate perfusion of avascular areas (Dammann et al, 2023). The presence of hypoxia-induced HIF-1α-dependent vascular endothelial growth factor (VEGF) stimulation predisposes vascular pathological changes, such as vascular leakage, vitreous hemorrhage, and angiogenesis, ultimately leading to retinal detachment and blindness in ROP (Broxterman and Hug, 2016).

Retinal hypoxia has been identified as the major stimulus that triggers pathological retinal neovascularization in the

✉ Peng Li, lipeng198610@163.com; ✉ Chuanxi Yang, 2205515@tongji.edu.cn
Peng Li, https://orcid.org/0000-0003-0365-2103; Chuanxi Yang, https://orcid.org/0000-0002-6970-1214

Received Mar. 27, 2025; Revision accepted May 15, 2025;
Crosschecked xxx. xx, 20xx; Published online xxx. xx, 20xx

© Zhejiang University Press 2025

development of ROP (Fevereiro-Martins et al, 2023). HIF-1, the oxygen-sensitive transcriptional activator, can orchestrate the process of angiogenesis by indirect cascade effects or direct binding to hypoxia-response elements (HREs) sites in the promoters of HIF-1 target encoding genes like *vegf* (Zimna and Kurpisz, 2015). Under hypoxic conditions, the continuous accumulation of stabilized HIF-1α could translocate into the nucleus and then activate the transcriptional transactivation of proangiogenic genes, while VEGF is the most potent promotor involved in angiogenesis among them (Rattner et al, 2019). Additionally, VEGF can also be secreted by hypoxia-induced microglial cells in the vitreous, contributing to the resultant disordered angiogenesis in the ROP (Rathi et al, 2017). Hence, VEGF has been widely studied as a potential therapeutic target for retinal pathological angiogenesis (Uemura et al, 2021).

At present, laser and sometimes cryotherapy are considered for treatment-warranted ROP, but they cause permanent retinal destruction (Mintz-Hittner et al, 2011). Additionally, intravitreal injections of the VEGF inhibitor bevacizumab have been reported to improve ROP (Chang et al, 2022). As the upstream master regulatory gene for VEGF, there are currently few effective therapeutics targeting HIF-1α activity available (Xu et al, 2018). Thus, given that hypoxia-induced activation of HIF-1α is an important cause of abnormal neovascularization in hypoxic retinal diseases (Rattner, et al, 2019), it is necessary to develop safe and valuable therapeutics for HIF-1α activity.

The pathogenetic actions of the renin-angiotensin system (RAS) have been evidenced to result in progressive alterations of various retinal vascular and neuro-glial diseases (Phipps et al, 2019). Ang-(1–7), a breakdown peptide hydrolyzed from angiotensin II (AngII), has been identified to inhibit the angiogenesis of various kinds of cancers by decreasing VEGF expression and attenuating hypoxia-stimulated cardiomyocyte apoptosis by inhibiting HIF-1α nuclear translocation (Chang et al, 2016; Domińska et al, 2018). As a novel vasoactive heptapeptide, Alamandine, directly generated from the decarboxylation of Ang-(1–7) (Lautner et al, 2013), was considered to share similar molecular sequence and biological properties with Ang-(1-7) by activating Mas-related G protein-coupled receptor D (MrgD) (Zhao et al, 2022a). Recently, expressions of MrgD receptors found in the retinal vasculature have also been reported to play a vital role in the retinal neurovascular function (Zhu et al, 2020). However, it remains unknown whether Alamandine could inhibit neovascularization in OIR.

Thus, in our study, we aimed to investigate the anti-angiogenic effects of Alamandine on hypoxia-induced retinal neovascularization and to further explore its occurrence mechanisms.

Unedited

2 Materials and methods

2.1 Analysis of single-cell transcriptomic data

Single-cell RNA sequencing (scRNA-seq) matrix data mainly from isolated retinal cells were obtained from GEO database (GSE283276; GSE173079; GSE243100; GSE150703), and scRNA-seq matrix data of fibrous membrane from proliferative vitreoretinopathy (PVR) or proliferative diabetic retinopathy (PDR) patients were obtained from GEO database (GSE165784; GSE245561) for further analysis (Hu et al, 2022). RAS-related gene set (GO: 0003081) were sourced from the Molecular Signatures Database (MSigDB). A comprehensive set of 25 Homo sapiens genes and 36 Mus musculus genes was retrieved for subsequent analyses. Then, Seurat package was used to conduct data analysis. Briefly, after mitigating batch efects and data normalization, uniform manifold approximation and projection (UMAP) was used to visual and identify refined cell clusters. The cell types were identified by established marker genes in different cell clusters.

2.2 Ethics approval and animal care

This study used C57BL/6J female mice and their pups (regardless of gender) purchased from the Vital River Corporation (Beijing, China). The experimental protocols gained approval from the Experimental Animal Care and Use Committee of Nanjing Medical University and were implemented in compliance with the Guidelines on the Care and Use of Laboratory Animals (NIH publication No. 85-23, revised 1996). Mice were housed on a circadian 12 h light-dark cycle (lights on at 07:00 am and off at 07:00 pm) and were permitted free access to food and water.

2.3 Animal model and treatment protocols

The mouse models of oxygen-induced retinopathy (OIR) are reproducible and quantifiable in terms of observing the progression of retinal neovascularization, making it a good model for mimicking ROP and examining the occurrence mechanisms underlying its pathogenesis (Rivera et al, 2016).

Newborn C57Bl/6J mice at postnatal day 7 (P7) were exposed to 75% oxygen for 5 consecutive days along with their mothers and were then returned to normal conditions (21% oxygen) from P12 to P17. Next, the retinas from OIR mice at P17 were obtained for further experiments.

2.4 Intravitreal injections

First, 0.5μl Alamandine (1.0μM/kg (Li et al, 2018); Synpeptide Co., Ltd., Shanghai, China) diluted in phosphate-buffered saline (PBS) was intravitreally injected using a 33-G needle and Hamilton syringe into each eye of the mice at P12. In another experiment, 0.5μl D-Pro^7-Ang-(1–7) (D-Pro^7; 1μM (Yang et al, 2020); Bachem, CA, USA) or A779 (10μM; Bachem (Yang, et al,

2020)) was intravitreally injected 3 hours before Alamandine. PBS was used as a control.

2.5 Immunofluorescent Staining

Flat mounts of the P17 retina were prepared according to Tual-Chalot et al.'s approach (Tual-Chalot et al, 2013). Concisely, both eyes were enucleated from euthanized neonatal mice and immersed in 4% PFA for 15 minutes at room temperature. Then, the retinas were carefully separated from surrounding tissues, radially cut using microscissors, and treated with cold methanol for 20 minutes or longer. Once the procedures above were finished, the retinas were washed gently with PBS containing 0.1% Tween-20, blocked with blocking solution containing 5% goat serum and 0.3% TritonX-100 diluted in PBS for 2 hours at room temperature, and probed with fluorescein-tagged isolectin B4 (1:150 diluted in blocking solution) overnight at 4°C. After rinsing with PBS 3 times, sections were mounted on Superfrost Plus slides, air-dried, and coverslipped with anti-fade mounting medium containing DAPI (Vector Laboratories, Burlingame, CA, USA). All fluorescence images were captured by a confocal laser scanning microscope (Carl Zeiss, Oberkochen, Germany).

2.6 Quantitation of retinal neovascularization in OIR mice

Retinal vaso-obliteration (RVO) and retinal neovascularization (RNV) were quantitatively analyzed as previously described (Zhao et al, 2022b). Briefly, the retinal whole-mount was stained with IB4 to label endothelial cells. Then, the images of whole-mount retinas were taken using a Zeiss fluorescence upright microscope (Carl Zeiss, Jena, Germany). Next, we quantified RVO and RNV by comparing the number of pixels in a given region to the total number of retinal pixels in images of whole-mount retinas of mice from different groups via Image-J software (The National Institute of Health, Bethesda, MD, USA). The new vessels that fluoresced more intensely than the surrounding normal vessels would be colored red (Connor et al, 2009).

2.7 Human retinal microvascular endothelial cell culture and treatment

Human retinal microvascular endothelial cells (HRMECs) (Angio-Proteomie; Boston, MA; CAP-0010) were cultured in endothelial cell medium (ECM) (ScienCell, Carlsbad, CA, USA) at 37 °C with 5% CO_2. To mimic the OIR model in vitro, HRMECs at passages 5 or 6 were placed in a homemade hypoxia incubator filled with 1% O_2, 5% CO_2, and 94% N_2 for 24 hours, as previously reported (Ahmed et al, 2016). In some experiments, HRMECs were preliminarily incubated with Alamandine (5μg/ml, 10μg/ml, 20μg/ml), D-Pro^7-Ang-(1–7) (D-Pro^7; 1μM; Bachem, CA, USA), or A779 (10μM, Bachem) for 30 minutes before hypoxia treatment. In some experiments, HRMECs were treated with 1μM Angiotensin II (Ang II) for 48 hours to induce a pathological model. All the cells were then subjected to the following studies.

2.8 Wound healing assay

To decipher the impact of Alamandine on cell migration capacity, HRMECs were cultured on 6-well plates before reaching a confluence of 90%. A pipette tip was utilized to artificially generate a straight wound. Live cell images were collected 24 hours after varying concentrations of Alamandine administration by a bright-field microscope and were processed with ImageJ software to calculate the wound width. A shorter width is routinely the consequence of a better migration rate of HRMECs.

2.9 Real-time cell analyzer proliferation and migration assays

A cell analyzer system constructed upon electrical impedance measurement offers a real-time means for recording the extent to which Alamandine alters the proliferation and migration status of HRMECs. To monitor the proliferation process, cells (2×10^3/well) were seeded in an E-plate 16 (ACEA Biosciences, San Diego, CA, USA), and 8 hours later, the cell suspension was transferred to serum-free medium with/without 10 ng/ml VEGF, with Alamandine being added at various concentrations. As for the migration assay, cells were seeded in a CIM-plate 16 (xCELLigence Roche, Penzberg, Germany) containing a serum-free medium. Each well of the lower chamber was filled with a certain concentration of Alamandine and 10 ng/ml VEGF to elicit chemotactic migration.

2.10 Aortic ring angiogenesis assay

The procedures for detecting ex vivo aortic angiogenesis with the Sprague–Dawley rats' aorta in our study were identical to previously established protocols (Nicosia and Ottinetti, 1990). After sacrifice, the thoracic aorta of rats was completely isolated and cut into 1-mm rings. Having been embedded in a 96-well plate (Corning, NY, USA) coated with Matrigel matrix, the aortic rings were then maintained in M119 medium supplemented with 2% FBS, VEGF (10 ng/ml), and Alamandine for 6 days. During this period, we renewed the growth medium at 2-day intervals. The degree of angiogenic sprouting from the aortic rings was microscopically inspected and photographed with a 10×objective, manually analyzed, and assigned a score ranging from 0 (least evident) to 5 (most evident) by a blinded investigator.

2.11 Tube formation assay for HRMECs

In vitro tube formation assay was conducted using a commercial tube formation kit (Cultrex, United States) following the

Unedited

manufacturer's guidance. HRMECs (2×10^4/well) were seeded in Matrigel matrix-coated 24-well plates (100μl/well). The cumulative amount and length of the tube were quantified with the assistance of ImageJ software.

2.12 Flow cytometry

The collected viable cells and cell debris were incubated with propidium iodide (PI) and Annexin-V (Fcmacs Biotech Co., China) in the binding buffer at room temperature for 30 minutes in darkness according to the manufacturer's instructions. Then, the flow cytometry method was applied to analyze the relative ratio of cell apoptosis.

2.13 Nuclear Proteins Extraction

The nuclear protein was extracted using the NucBuster™ protein extraction kit (Novagen®, Rockland, DE, USA), according to the manufacturer's protocol.

2.14 Western blotting

The total protein of HRMECs and retinas was isolated with radioimmunoprecipitation (RIPA) lysis buffer (containing phosphatase and protease inhibitor cocktails), with the protein concentration being measured using a BCA Protein Assay Kit (Pierce, Rockford, IL, USA). Approximately 30–50 μg of protein of each sample was loaded for 10% sodium dodecyl sulfate-polyacrylamide gel electrophoresis (SDS-PAGE) and was subsequently transferred onto polyvinylidene difluoride (PVDF) membranes (Millipore, Bedford, MA, USA). A 5% BSA solution was prepared for blocking non-specific binding. Membranes were incubated with primary antibodies overnight at 4℃, followed by incubation with horseradish peroxidase-conjugated secondary antibodies at room temperature for 2 hours. After three washes with Tris-buffered saline with Tween-20 (TBST), protein bands were visualized with enhanced chemiluminescence reagent, with band densities being quantified using ImageJ software. To compare the protein levels among different samples, β-Actin was used as an internal reference. Primary antibodies used were as follows: caspase 3 (1:1000, #14220; Cell Signaling Technology, MA, United States), cleaved-caspase 3 (1:1000, #9664; Cell Signaling Technology), Bax (1:1000, #5023; Cell Signaling Technology), Bcl2 (1:1000, #15071; Cell Signaling Technology), HIF-1α (#36169; Cell Signaling Technology, USA), VEGF (No.19003-1-AP; Proteintech Co., Wuhan, China), PCNA (No.10205-2-AP; Proteintech Co., Wuhan, China), MrgD (1:1000; Abcam), eNOS (1:1000, #32027; Cell Signaling Technology), and iNOS (No.22226-1-AP; Proteintech Co., Wuhan, China).

2.15 Quantitative real-time PCR

Total RNA extraction from cells or tissues was performed using the Trizol reagent (Invitrogen, Carlsbad, CA, USA). After examining RNA concentration and purity using a Nanodrop-1a000 spectrophotometer (Thermo Scientific, Wilmington, DE, USA), a PrimeScript RT reagent kit (Takara Bio, Otsu, Japan) was applied for generating reverse-transcribed cDNA. An SYBR green-based quantitative real-time PCR (qRT-PCR) assay was conducted on an ABI Prism 7000 sequence detection system (Applied Biosystems, Foster City, CA, USA) to detect mRNA expression. Relative gene expression was determined using the $2^{-\Delta\Delta Ct}$ method and was normalized to the internal control gene GADPH. For miRNA quantification, the BulgeLoopTM miRNA Reverse Transcription Kit (RiboBio, Guangzhou, China), the Bulge- LoopTM miRNA qRT-PCR Starter Kit (RiboBio, Guangzhou, China), and miRNA-specific primers (RiboBio, Guangzhou, China) were used, with GAPDH serving as an endogenous control. The primer sequences used in this study were illustrated item by item in Table S1.

2.16 Liquid chromatography-mass spectrometry

We performed Liquid chromatography-mass spectrometry (LC-MS/MS) to identify the metabolites of the retinas or serum of the mice from the normoxia and hypoxia groups. First, we extracted the metabolites from the retinas via 80% CH3OH/Milli-Q water. Then, the dried samples were transferred to autosampler vials for LC-MS analysis (n=6). Briefly, reversed-phase LC (HP1100, Agilent Technologies, Santa Clara, CA, USA) was used to separate the metabolites. Next, each sample was injected into the C18 column for analysis. Finally, data analysis was performed using the XCMS Online at https://xcmsonline.scripps.edu/.

2.17 Statistical analysis

Data are expressed as mean±standard error of the mean (SEM). One-way analysis of variance (ANOVA) followed by Bonferroni's post hoc test was performed to evaluate the significance of multigroup mean differences. Values were considered statistically significant for $P < 0.05$. All the data were analyzed using GraphPad Prism 7.0 software (GraphPad Inc., San Diego, CA, USA).

3 Results

3.1 scRNA-seq data integration and clustering

We first integrated scRNA-seq data (including GSE165784 and GSE245561) of fibrous membrane from PVD or PDR patients via Harmoney, scVI and Seurat analysis methods (Fig. 1a). Based on the Seurat method, which provided the most

Unedited

competitive results, 7 different color-coded cell types were annotated in Seurat UMAP clustering plot, and their proportions in the PDR and PVR samples were also represented in a bar graph (Fig. 1b). Next, a comprehensive gene set of 25 Homo sapiens genes and 36 Mus musculus genes, termed RASGs, was retrieved from the MSigDB database for subsequent analyses, so as to investigate the possible relationship between RAS and PDR. The average gene expression of RASGs in distinct cell types was visualized in Heat map, Violin plot and UMAP clustering plot (Fig. 1c-e). The results showed that RASGs expressed highest in the Microglial cells, and Endothelial cells (ECs) subsets. Considering the reported value of ECs in the development of pathological retinal neovascularization (Huang, 2020), we further clustered ECs subset into 6 subclusters (VEC1-6) to explore its distribution pattern (Fig. 1f). The subclusters were scored in accordance with RASGs expression, and their gene expression profiles were showed in Fig. 1g-h. Furthermore, we integrated single-cell RNA sequencing data (including GSE283276, GSE173079, GSE243100 and GSE150703) of isolated retinal cells from OIR, PDR and Control mice model. The Seurat UMAP clustering plot showed 12 different color-coded cell types (Fig. 2a-b). The average gene expression of RASGs in distinct cell types was also visualized (Fig. 2c-e), and the expression of RASGs was highest in the Microglial cells, ECs and Pericyte cells subsets. The gene expression profiles of 5 subclusters scored according to RASGs expression were shown in Fig. 2f-h. By integrating transcriptomic data across multiple species, we identified that RAS-associated ECs populations were indeed highly related to retinal neovascularization, establishing a foundation for developing targeted therapeutic strategies that modulate RAS activity to mitigate pathological neovascularization. Thus, we further explored the possible role of RAS towards ECs dysfunction.

3.2 LC–MS-mediated metabolomics analysis of OIR mouse model

To explore the occurrence mechanisms of ROP, we first established the OIR mouse model in vivo. Then, based on the role of the high-throughput LC-MS/MS method in revealing mechanisms and therapeutic targets for different diseases, we performed the LC-MS/MS method to qualitatively analyze the different compounds of RAS system in serum and retina tissues between the OIR and control groups to explore the novel mechanisms of ROP development. The results showed that the heptapeptide Alamandine in serum and retinas is significantly decreased in OIR mice compared with the control group (Fig. 3a-b).

Alamandine, generated from catalytic hydrolysis of Ang A via ACE2, is a novel member involved in the ACE2/Ang-(1–7)/Mas protective axis in the renin–angiotensin system. Due to the different expression of Alamandine in serum and retinas between the OIR and control groups, we next detected some other vital RAS members that are involved in the generation of Alamandine. Compared with the control group, our analysis of LC-MS/MS data in the OIR group showed higher levels of angiotensin II (AngII) (Fig. 3c-d) and lower levels of ACE2 (Fig. 3e-f) in serum and retinas. Moreover, ACE, AGT, and AT2 mRNA expression levels were lower in hypoxia-induced HRMECs versus control (Fig. S1a). The above LC-MS/MS results suggested that the expression of RAS members, especially the novel polypeptide Alamandine, may be affected during the occurrence and progression of ROP. Considering that the expression of MrgD, the natural receptor of Alamandine, has also recently been reported to play a crucial role in retinal neurovascular function (Zhu, et al, 2020), we were eager to further explore the possible role of Alamandine in the development of ROP.

3.3 Effects of Alamandine on VEGF-induced Angiogenesis in HRMECs

To investigate the potential values of Alamandine in angiogenesis in vitro, further studies were conducted on VEGF-mediated angiogenesis in HRMECs. First, the results of flow cytometry showed that there was no statistical significance between different groups, meaning that different concentrations (5, 10, 20μg/mL) of Alamandine have no evident pro-apoptotic effects on cultured HRMECs (Fig. 4a). Subsequent RTCA assays showed that Alamandine could significantly attenuate VEGF-induced endothelial cell (EC) migration and proliferation in a dose-dependent manner (Fig. 4b-c). Since pathological angiogenesis is characterized by EC migration, tube formation, and microvascular sprout induced by VEGF or a hypoxic microenvironment, wound healing assay, tube-formation assay, and aortic rings assay were further carried out to confirm the role of Alamandine in ex-vivo angiogenesis in HRMECs. As shown in Fig. 4d-e, Alamandine could dose-dependently inhibit VEGF-induced closure of the scratch wound and capillary-like tube formation. In addition, the numbers and morphology of new growth sprouts surrounding the aortic rings showed that VEGF promoted microvascular sprouting and blood vessel network formation, which could be suppressed by Alamandine treatment dose-dependently (Fig. 4f). We also found that Alamandine ameliorated Ang II-induced EC apoptosis, migration, and proliferation (Fig. S2a-c). Collectively, these results indicated that Alamandine did prevent VEGF-induced angiogenesis in vitro.

3.4 Effects of Alamandine on hypoxia-induced HIF-1α/VEGF pathway activation and apoptosis in HRMECs

Next, we investigated the expression of the HIF-1α-VEGF pathway, which has been reported to play a crucial role in continuous inflammatory infiltration involved in hypoxia-induced microvascular angiogenesis. As shown in Fig. 5a-b, hypoxia could increase mRNA expression of VEGF in HRMECs, and then 10μg/ml Alamandine was chosen as the most suitable concentration for further experiments. Next, the protein expression levels of HIF-1a, VEGF, and CC3, as well as the ratio of Bax/Bcl2, were increased after 24h of hypoxia induction in HRMECs; however, they were inhibited by Alamandine treatment (Fig. 5c-g). The above results suggested that Alamandine could prevent hypoxia-induced apoptosis and activation of the HIF-1α-VEGF

Unedited

pathway in vitro, which could be supported by further immunofluorescence results of HRMECs staining with HIF-1a or CC3, respectively (Fig. 5h-k). The Western blot results also showed that Alamandine dramatically inhibited hypoxia-induced nuclear import of HIF-1α in vitro (Fig. 6l). Next, HIF-1α stabilizer dimethyloxalylglycine (DMOG) hindered the inhibitory effects of Alamandine on hypoxia-induced VEGFA and PCNA (Fig. 5m).

3.5 Effects of Alamandine on pathological neovascularization in the retinas of OIR mice

To further investigate the role of Alamandine in regulating retinal neovascularization in OIR mouse models, retinal paraffin sections staining with HE and whole-mount immunostaining with IB4 were performed on day 17 (Fig. 6a-b). As shown in the high-resolution images, the increased number of hypoxia-stimulated pre-retinal neovascular cell nuclei penetrating the internal limiting membrane (ILM) in the OIR group was decreased by the Alamandine treatment. Additionally, the percentages of neovascular tufts areas (Fig. 6c) and neovascular areas (Fig. 6d), as well as the ratio of avascular areas to total areas (Fig. 6e), were increased in mouse retinas from the OIR group compared with the control group, which were reduced after intravitreal injection of Alamandine. Notably, Alamandine alone has no significant adverse effects on retinal vessel development in a normal retina (Fig. S4). These data indicated that Alamandine could dramatically improve hypoxia-induced retinal pathological neovascularization and physiologic revascularization in mouse models of OIR.

3.6 Effects of Alamandine on vessel proliferation and HIF-1α/VEGF pathway activation in the retinas of OIR mice

Since hypoxia-induced VEGF favors angiogenesis and vasoproliferation, which can result in abnormal neovascularization (Rattner, et al, 2019), we used PCNA as a proliferation marker to examine the proliferation capacity of vessel ECs in vivo. The OIR-induced protein expression of PCNA in retinas was significantly decreased by Alamandine (Fig. 6f). In agreement with Western blot results, the density of PCNA-positive cells was increased within the retinal neovessels in the OIR group compared with that in the control group, which was decreased after the administration of Alamandine (Fig. 6g). Then, we examined whether the HIF-1α/VEGF pathway was also involved in the beneficial effects of Alamandine in vivo models. Western blot results showed that hypoxia-induced HIF-1α and VEGF protein expression in retinal tissues from the OIR group was significantly decreased after Alamandine treatment. The same trend was found in the mRNA expression of HIF-1α (Fig. 6h) and VEGF (Fig. 6i) in vivo. Consistent with the above Western blot and PCR results, the immunofluorescence intensities of HIF-1α or VEGF-positive cells in mouse retinal paraffin sections from the OIR group were raised compared with those of the control group and were reduced in Alamandine-treated OIR mice (Fig. 6j). The above results revealed that Alamandine could inhibit vessel proliferation and activation of the HIF-1α/VEGF pathway, thereby attenuating OIR-induced pathological retinal neovascularization.

Unverified

3.7 Effects of Alamandine on glial cells dysfunction and inflammation in the retinas of OIR mice

The indispensable role of retinal glial cell function has been reported to regulate the integrity of retinal vasculature involved in the pathological retinal angiogenesis of ROP. To determine the effects of Alamandine on hypoxia-induced retinal glial cell dysfunction in OIR mouse models, we used immunofluorescence-specific antibodies GFAP and Iba1 to label astrocytes and microglial cells in mouse retinas, respectively. As shown in Fig. 7a, compared with the control group, an OIR-induced drop in astrocyte density was observed in both retinal avascular and neovascular areas. Unlike the uniform distribution of astrocytes in the retinas of the control group, their distribution in the OIR group was destroyed by hypoxic injury. However, Alamandine treatment could restore the normal density and distribution of astrocytes in OIR retinas. In addition, the immunofluorescence intensity of activated retinal microglia in the OIR group was increased compared with the control group, which was reduced after the administration of Alamandine in OIR-treated mice (Fig. 7b).

Considering that retinal glial cell dysfunction can lead to the excessive production of pro-inflammatory cytokines (Au and Ma, 2022), we investigated the effects of Alamandine on the OIR-induced release of pro-inflammatory cytokines. As shown in Fig. 7c, the mRNA expression of IL-1β, IL-6, TNF-α, MCP-1, MMP-9, and COX-2, as well as ICAM-1 and VCAM-1, were all upregulated in retinal tissues from the OIR group, and Alamandine treatment could downregulate OIR-induced elevations of the above pro-inflammatory cytokines. Meanwhile, Western blot results showed that the protein expression of oxidative stress-associated iNOS and eNOS was increased in the retinas of the OIR group and was decreased after administration of Alamandine (Fig. 7d-e). These results indicated that Alamandine could improve OIR-induced retinal glial cell dysfunction and inflammation.

3.8 Role of MrgD in the protective effects of Alamandine against hypoxia-induced pathological angiogenesis

Alamandine has been reported to exert bioactive effects via its endogenous receptor MrgD (Schleifenbaum, 2019). In our study, Alamandine treatment could increase the protein expression of MrgD in HRMECs time-dependently (Fig. S4a-b). Next, we investigated the role of MrgD in the beneficial effects of Alamandine on pathological angiogenesis. In vitro, coincubation with D-Pro^7 (MrgD and Mas receptor antagonist), but not with A-779 (specific Mas receptor antagonist) or PD123319 (AT2R inhibitor), could block the downregulation of HIF-1α and VEGF induced by Alamandine in hypoxia-treated HRMECs (Fig. S4c-d). In vivo, mouse models were pre-treated with D-Pro^7, PD123319, or A-779 in the presence of hypoxia and Alamandine. As shown in Fig.

8a-d, pre-treatment with D-Pro^7 could reverse the protective effects of Alamandine against OIR-induced retinal avascular zones and neovascularization tufts, while A-779 failed. Corroborating this finding, the same trend was also found in the protein expression of HIF-1α and VEGFA (Fig. 8e). Accordingly, we could infer that Alamandine did play an anti-angiogenesis role through the HIF-1α/VEGF pathway via MrgD in hypoxia-induced pathological angiogenesis.

3.9 Role of MrgD in the protective effects of Alamandine against glial cells dysfunction and inflammation in the retinas of OIR mice

We next investigated the participation of the MrgD receptor in Alamandine's effects on OIR-induced retinal glial cell dysfunction and inflammation. As shown in Fig. S5a, D-Pro^7 pre-treatment could counteract the actions of Alamandine in downregulating OIR-induced mRNA expression of various pro-inflammatory cytokines, including IL-1β, IL-6, TNF-α, MCP-1, COX-2, and MMP9, as well as ICAM-1 and VCAM-1 in the retinas. Also, the protective effects of Alamandine on restoring the normal density and distribution of retinal astrocytes and microglial cells in the OIR-treated mouse were inhibited by D-Pro^7 pre-treatment (Fig. S5b-c). Taken together, the above studies indicated that Alamandine could improve OIR-induced retinal glial cell dysfunction and inflammation, thus attenuating pathological angiogenesis by regulating the HIF-1α/VEGF pathway via MrgD.

4 Discussion

To our knowledge, this work proved for the first time that Alamandine has a protective role in improving hypoxia-induced retinal microvascular dysfunction and pathological neovascularization by inhibiting the activation of the HIF-1α/VEGF pathway via MrgD in OIR mice.

Considering the similar pathogenesis and pathological features, the tested mouse models of OIR have been widely used to resemble ROP for their convenience in terms of observation, which allows us to explore the potential molecular mechanisms (Rivera, et al, 2016). ROP (initially termed retrolental fibroplasia) is an ischemia-induced proliferative retinal vasculopathy that occurs in premature infants, ultimately causing vision impairment and even blindness (Daruich et al, 2020). As ROP progresses, various hypoxia-induced pathological changes, including but not limited to blood–retinal barrier (BRB) damage, vascular hyperpermeability, and inflammation, have been identified to facilitate the formation of intravitreal neovascular tufts through activating HIF-1α-dependent VEGF activity and other signaling pathways (Broxterman and Hug, 2016; Guo et al, 2020).

Various cell types which consisted of retina exerted their distinct effects in retinal pathological conditions (Voigt et al, 2021), which remained to be fully elucidated. Emerging evidence from scRNA-seq studies has revolutionized our understanding of ECs heterogeneity and their functional contributions to retinal neovascularization progression (Cheng et al, 2024; He et al, 2024), thereby providing critical insights for therapeutic targeting. The integration of multi-species scRNA-seq data in our study represented a paradigm shift in retinal vascular biology research, significantly enhancing both the scientific rigor and translational relevance of our study on retinal neovascularization. Here, we did also find that ECs were highly related to retinal neovascularization via scRNA seq data analysis. Besides, the cell-type-specific signatures identified through scRNA-seq could guide the development of precision therapies (Au and Ma, 2022; Zhang et al, 2024). For instance, EC clusters with high angiogenic factor 1 with a G patch and FHA domain (AGGF1) expression related to advanced retinal neovascularization stages (Cheng et al, 2025). In our study, we found that RAS-associated ECs may respond to retinal neovascularization as well.

RAS played a pivotal role in regulating ECs function during various diseases (Moravski et al, 2003; Amraei and Rahimi, 2020). Multiple biological compounds involved in the RAS are widely expressed in the retina (Paul et al, 2006). Notably, genetically engineered mice have elucidated the causal role of RAS in retinal pathological neovascularization. For example, previous study has revealed that EC-specific deletion of adenosine A2a receptor ($A_{2a}R$) improved OIR-induced retinal angiogenesis in mice (Santiago et al, 2020). RAS-targeted therapies, including small-molecule inhibitors, could suppress hypoxia-driven angiogenesis, underscoring its pathological role (Boddu et al, 2023). Changes in the expression levels of serum RAS members, including Ang-1 and Ang-2, may be promising biomarkers for reflecting the regression and treatment of ROP (Yang et al, 2021; Wang et al, 2023). Among them, serum Ang-(1–7) levels have also been demonstrated to predict the development of retinopathy in diabetics (Duan et al, 2018). Ang-(1–7) has been reported to exert anti-angiogenic and anti-apoptosis effects by inhibiting VEGF activation and HIF-1α nuclear translocation, respectively (de Carvalho Santuchi et al, 2019). It can also play a beneficial role in cardiovascular diseases by interacting with MrgD, which is a natural endogenous receptor of Alamandine. Notably, the expression of MrgD has recently been reported to play a crucial role in retinal neurovascular function (Zhu, et al, 2020). As the novel members are involved in the counter-regulatory mechanism within the RAS, the similar molecular structures and receptors between Alamandine and Ang-(1–7) may account for their similar protective actions (Schleifenbaum, 2019). Thus, we used the LC-MS/MS method to explore the possible changes in Alamandine and some other RAS members related to the generation of Alamandine in the retina and serum and further investigated a new possible mechanism in the treatment of ROP. In our initial studies, lower expression levels of Alamandine and higher levels of AngII in serum and retinas were found in ROP infants compared with their age-matched healthy subjects through the LC-MS/MS method. Thus,

Unedited

further investigations were undertaken to examine whether Alamandine could inhibit OIR-induced angiogenesis. Our data showed that Alamandine could attenuate VEGF- or hypoxia-induced HRMEC proliferation, microvascular sprouting, and migration, meaning that it can reduce pathological angiogenesis in neovascular areas. Moreover, Alamandine improved hypoxia-induced retinal neovascularization and vascular dysfunction in mouse models of OIR dose-dependently.

In the process of vascular invasion involved in the formation of neovessels with functional defects and structural abnormalities, the endoproteases MMPs have been reported to play a critical role in vitreous leakage and hemorrhage (Choręziak-Michalak et al, 2023). In our study, in agreement with the presence of increased MMP expression reported in the vitreous of ROP patients (Rathi, et al, 2017), elevated levels of MMP9 after hypoxia stimulation were found in vivo and in vitro, which can be decreased by Alamandine treatment.

Retinal hemorrhage found in ROP indicates the presence of a disrupted and hyperpermeable vascular barrier system consisting of retinal glial cells (Hartnett, 2023). Regarding the reported indispensable and mutually reinforcing relationships between pathologic retinal angiogenesis and retinal glial dysfunction during pathological development in mouse models of OIR, since Alamandine could attenuate hypoxia-induced neovascularization, it may also be able to restore the integrity of retinal vasculature (Karlstetter et al, 2015). As the variants of macroglia, both astrocytes and Miiller cells are involved in the normal development of the retinal vessels by wrapping around retinal ganglion cells' axon bundles that are essential for the formation of the blood–retina barrier (Li et al, 2019). It has been established that the hypoxia-induced distribution of retinal astrocytes located within the nerve fiber layer from the optic disc into vascularized retinas could result in the disorderly formation of neovascular tufts in the avascular area of ROP (Perelli et al, 2021). Additionally, the oxygen-induced injury may induce astrocytes to secret VEGF, contributing to pathological neovascularization (Rathi, et al, 2017). GFAP (glial fibrillary acidic protein)-like immunoreactivity is well-recognized to label astrocytes in the retina, making it viable for further studies (Brenner and Messing, 2021). In our study, Alamandine treatment could significantly reduce newly induced vessels and vascular leakage in the remodeling retinal zone of OIR by restoring the normal density and distribution of astrocytes.

In the case of oxygen-induced injury, activated microglia cells have also been evidenced to cluster around retinal neovessels in a disorderly manner and produce excessive pro-inflammatory cytokines, including TNF-α, IL-1β, IL-6, and MCP-1, thus promoting the pathological progression of OIR in mouse models (Checchin et al, 2006; Aouiss et al, 2019). Then, the increased inflammation may contribute to the potentiated oxidative stress, resulting in the uncoupling of eNOS and the decreased release of nitric oxide (NO) derived from eNOS in the vasculature (Li et al, 2014). Similar to Ang-(1-7), Alamandine has also been demonstrated to have anti-inflammatory and anti-proliferation effects on cardiovascular diseases by regulating the pro-inflammatory signaling cascade, and NO production responded to pathological stimulus in cardiomyocytes and endothelial cells via interacting with the MrgD receptor (de Jesus et al, 2018; Zhao et al, 2022a). In our study, Alamandine treatment could inhibit the migration and activation of microglia cells, accompanied by the reduced production of pro-inflammatory cytokines in the OIR. These data could also support the notion that Alamandine inhibits OIR-induced microvascular injury and pathological angiogenesis by suppressing inflammation and oxidative stress.

In response to hypoxia-activated oxidative stress and immune response in endothelial cells, multiple related signaling pathways are activated, among which the HIF-1α-VEGF pathway has been suggested as the most crucial (Zhao et al, 2023). It has been reported that hypoxia-induced HIF-1α-dependent VEGF stimulation is most closely related to hypoxia-induced retinal neovascularization in ROP (Dong et al., 2021; Zhao et al., 2022b). Under hypoxic or anaerobic conditions, HIF-1α becomes stable. After being translocated into the nucleus, accumulated HIF-1α dimerizes with the HIF-1β subunit, which is essential for the emergence of endothelial cells during the embryonic period (Rattner, et al, 2019). Then, the HIF-1α/β dimer promotes vasculogenesis by activating the transcriptional activity of the proangiogenic genes like *vegf* (Vallée et al, 2018). VEGF, the most important factor that favors vast proliferation and angiogenesis, is secreted by hypoxia-induced microglial cells, leading to abnormal neovascularization in mouse models of OIR (Lashkari et al, 2000; Rathi, et al, 2017). In our study, Alamandine treatment could reduce hypoxia-induced nuclear import of HIF-1α, as well as the expression of the HIF-1α and VEGF of HRMECs, suggesting that Alamandine exerts its protective effects against ROP through inactivating the HIF-1α-VEGF pathway.

MrgD, also called TGR7, is one of the members of the GPCR family that plays a crucial role in regulating the inflammation and vascular endothelium function involved in the pathophysiological development of cardiovascular remodeling (de Jesus et al, 2023). Several previous studies have reported that Alamandine could elicit its bioactive effects in the cardiovascular system by activating the MrgD receptor (Lautner, et al, 2013; Schleifenbaum, 2019; Zhao, et al, 2023). Interestingly, Alamandine treatment was demonstrated to improve vascular fibrosis via upregulating MrgD expression (Yang, et al, 2020). Also, we previously reported that Alamandine alone could stimulate MrgD expression in primary neonatal rat cardiomyocytes (NRCM) and primary neonatal rat fibroblasts (NRCF) (Zhao, et al, 2023). More importantly, while losartan upregulated the levels of its receptor AT1R in the left ventricle in a negative feedback manner (Song et al, 2015), Alamandine was deemed an MrgD blocker that elevated MrgD expression in a negative feedback manner (Zhao, et al, 2023). In our study, we found that Alamandine treatment upregulated MrgD expression in vivo and in vitro.

Since the Alamandine/MrgD axis has been considered a novel protective mechanism against retinal diseases (Zhu, et al, 2020), we speculated that Alamandine may inhibit hypoxia-induced pathological angiogenesis via MrgD. As an AT2R inhibitor,

Unedited

PD123319 is also regarded as an MrgD receptor antagonist, which can attenuate the protective effects of Alamandine or Ang-(1-7) in some studies, but not all (Park et al, 2018). Additionally, D-Pro^7-Ang-(1-7) (D-Pro^7) can block the binding of Alamandine to the MrgD receptor and Mas receptor by way of competitive inhibition. It has been evidenced that the cardioprotective actions of Alamandine can be blocked by pre-treatment with D-Pro^7(Park, et al, 2018). In our study, the beneficial role of Alamandine in inhibiting hypoxia-induced activation of the HIF-1α/VEGF pathway was reversed after coincubation with D-Pro^7 but not with PD123319. However, the inhibitory effects of Alamandine on MAPK and PI3K/AKT/mTOR signaling pathways were not blocked. Furthermore, the protective effects of Alamandine on improving hypoxia- or VEGF-induced HRMECs proliferation, microvascular sprouting, and migration were not abolished by pre-treatment with the specific Mas receptor antagonist, A-779, suggesting that Alamandine did exert its anti-angiogenesis effects by regulating the HIF-1α/VEGF pathway via MrgD.

5 Conclusions

Taken together, this work integrally demonstrated that Alamandine could improve hypoxia-induced retinal vascular barrier dysfunction with a restored glial cell network and alleviated inflammation response. Thus, it inhibits retinal pathological neovascularization by inhibiting the HIF-1α/VEGF pathway via MrgD in OIR mice models, paving the way for future clinical application of Alamandine in ROP.

Data availability statement

All data supporting the findings of this study are available within the paper and its Supplementary Information.

Acknowledgments

This work is supported by the Youth Program of the National Natural Science Foundation of China (82200379&82300309), the Shanghai Sailing Program (22YF1443100), the Academy talent special fund of The First Affiliated Hospital of Nanjing Medical University (YNRCQN0312&MXJL202208), and the Jiangsu Funding Program for Excellent Postdoctoral Talent (2023ZB592).

Author contributions

Kun ZHAO conceived the study, coordinated the scientific team, and allocated the funding for the project; Yaping JIANG performed the experimental research and data analysis; Wen HUANG performed the establishment of animal models; Yukang MAO wrote and edited the manuscript; Yihui CHEN conceived the study; Peng LI coordinated the scientific team, and reviewed the manuscript; Chuanxi YANG conceived the study, coordinated the scientific team, and allocated the funding for the project. All authors read and approved the final manuscript and, therefore, had full access to all the data in the study and take responsibility for the integrity and security of the data.

Compliance with ethics guidelines

All authors declare that they have no conflict of interest.

The experimental protocols have gained approval from the Experimental Animal Care and Use Committee of Nanjing Medical University, and were implemented in compliance with the Guidelines on the Care and Use of Laboratory Animals (NIH publication No. 85-23, revised 1996).

Figure and Table:

Table 1 List of utilized primers for qRT-PCR

Gene	Species	Forward primer	Reverse primer
VEGF	Human	GCAGAAGGAGGAGGGCAG	CACCAGGGTCTCGATTGGAT
HIF-1α	Human	CGGAAACTGAAGACCAACAAC	CAGAGGCAGGTAATGGAGACA
IL-1β	Human	ATGATGGCTTATTACAGTGGCAA	GTCGGAGATTCGTAGCTGGA
IL-6	Human	ACTCACCTCTTCAGAACGAATTG	CCATCTTTGGAAGGTTCAGGTTG
TNF-α	Human	GAGGCCAAGCCCTGGTATG	CGGGCCGATTGATCTCAGC
MCP-1	Human	CTCAGCCAGATGCAGTTAATG	TCTCCAGCCGACTCATTGG
ICAM-1	Human	ATGCCCAGACATCTGTGTCC	GGGGTCTCTATGCCCAACAA
VCAM-1	Human	GGGAAGATGGTCGTGATCCTT	TCTGGGGTGGTCTCGATTTTA
MMP9	Human	TGTACCGCTATGGTTACACTCG	GGCAGGGACAGTTGCTTCT
ACE	Human	GGGAAAGGCACTACCATGTCG	GGTGAGTTGTTGTCTGGCTTC
AGT	Human	TCCAGACTCCGATCATCAAGC	GCTCATGGTGTTCAGAATTGTGT
AT1	Human	CCCCAGTCTGAGATGGCTC	GACGAGGTGGAAGGGGTGTA
GAPDH	Human	GGAGCGAGATCCCTCCAAAAT	GGCTGTTGTCATACTTCTCATGG

Unedited

VEGF	Mice	CTGCCGTCCGATTGAGACC	CCCCTCCTTGTACCACTGTC
HIF-1α	Mice	ACCTTCATCGGAAACTCCAAAG	CTGTTAGGCTGGGAAAAGTTAGG
GAPDH	Mice	CCTCGCCTTTGCCGATCC	GGATCTTCATGAGGTAGTCAGTC

Fig. 1 Analysis of single-cell transcriptomic data in human

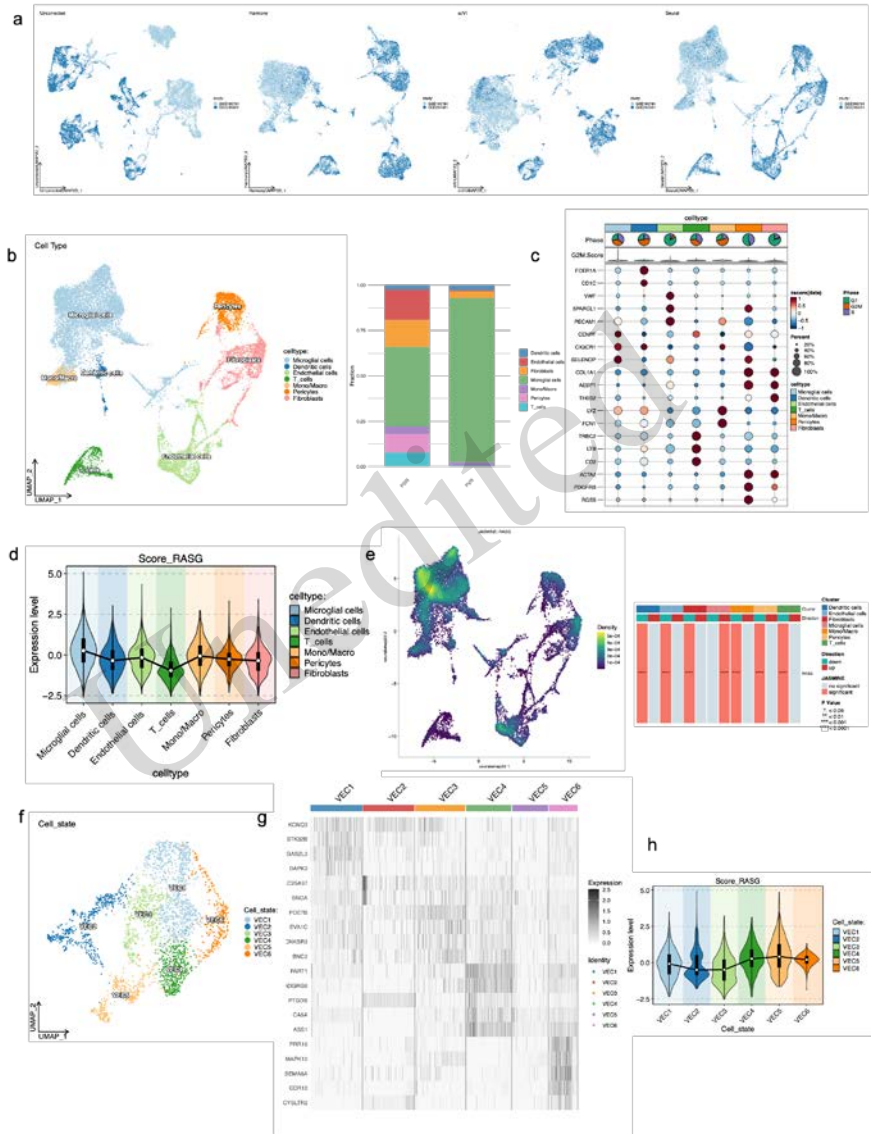

(a) The uncorrected and three types of re-clustered UMAP (uniform manifold approximation and projection) clustering of single-cell transcriptomic data from GEO datasets; (b) Seurat UMAP clustering of cell types (left) and its bar graph (right); (c) Heat map of expression levels of RASG (Renin-angiotensin system-related gene set) genes in key cell types of isolated retinal cells; (d) Violin plot of expression levels of RASG genes in key cell types of isolated retinal cells from PVD (proliferative vitreoretinopathy) and PDR (proliferative diabetic retinopathy) patients; (e) UMAP of density scores of the RASG gene set in different cell types; and its visualized bar graph. (f) UMAP plots of 5 clusters in endothelial cells; (g) Heap map of leading 3 signature gene expression profiles for the 6 endothelial cells clusters; (h) expression scores of RASG genes in 6 endothelial cells clusters.

Fig. 2 Analysis of single-cell transcriptomic data in mice

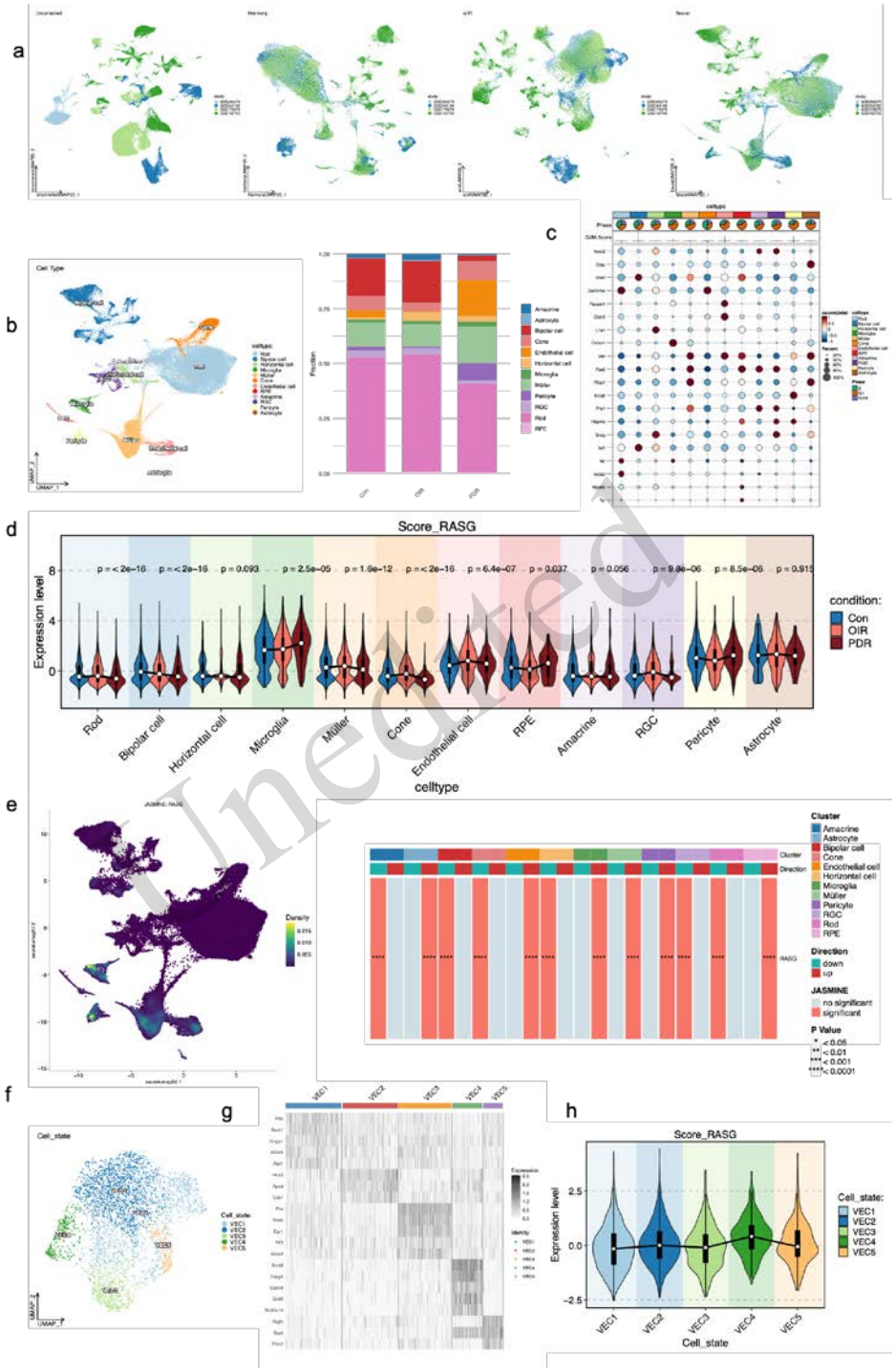

Unedited

(a) The uncorrected and three types of re-clustered UMAP (uniform manifold approximation and projection) clustering of single-cell transcriptomic data from GEO datasets; (b) Seurat UMAP clustering of cell types (left) and its bar graph (right); (c) Heat map of expression levels of RASG (Renin-angiotensin system-related gene set) genes in key cell types of isolated retinal cells; (d) Violin plot of expression levels of RASG genes in key cell types of isolated retinal cells from OIR (oxygen-induced retinopathy), PDR (proliferative diabetic retinopathy) or Control mice models; (e) UMAP of density scores of the RASG gene set in different cell types; and its visualized bar graph. (f) UMAP plots of 5 clusters in endothelial cells; (g) Heap map of leading 3 signature gene expression profiles for the 5 endothelial cells clusters; (h) expression scores of RASG genes in 5 endothelial cells clusters.

Fig. 3 LC–MS-mediated metabolomics analysis of OIR mouse model.

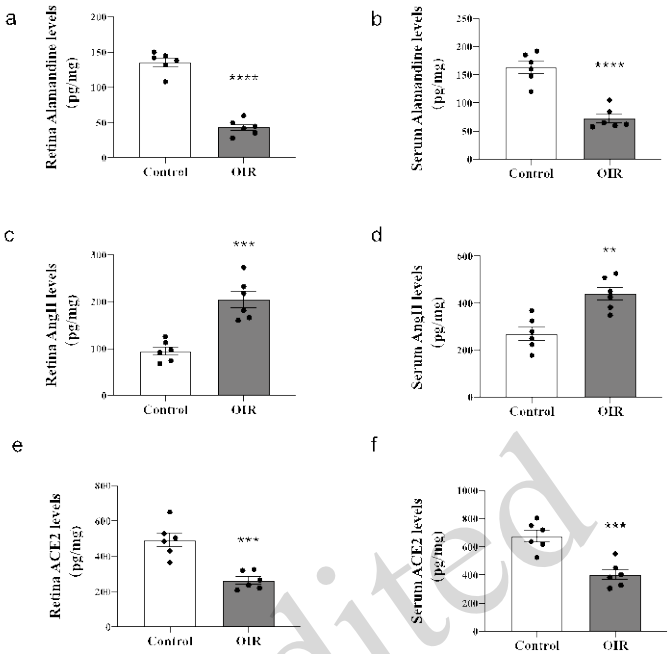

a-b, the high-throughput LC-MS/MS qualitatively analyzed Alamandine in serum (a) and retina (b) tissues between the OIR and control groups. c-f, the high-throughput LC-MS/MS qualitatively analyzed angiotensin II (c-d) and ACE2 (e-f) in serum and retina tissues between the OIR and control groups. All the results are expressed as mean ± SEM (n=6 per group; **P<0.01, ***P<0.001, ****P<0.0001, compared with the control group).

Fig. 4 Effects of Alamandine on VEGF-induced angiogenesis in HRMECs.

Unedited

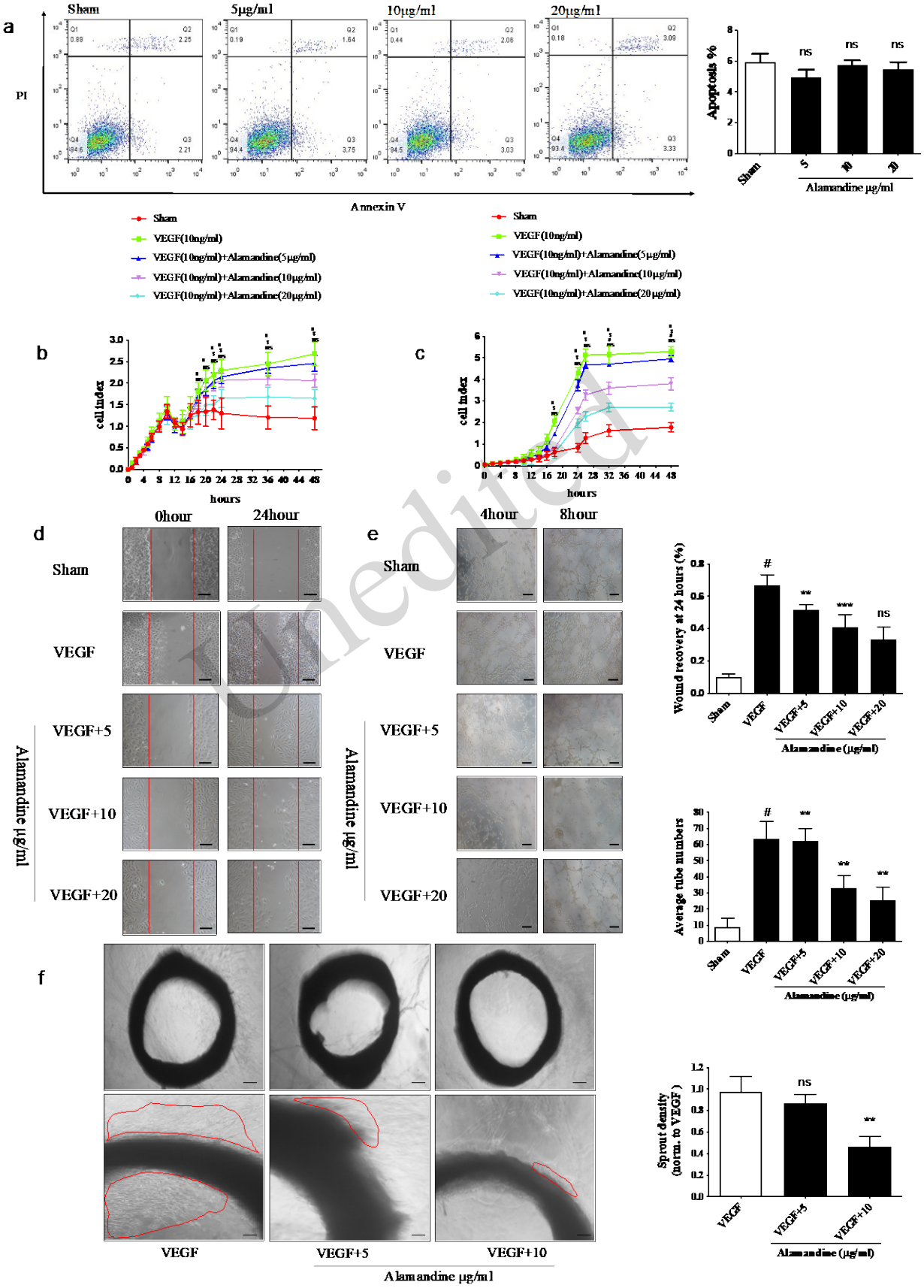
a
Sham
5μg/ml
10μg/ml
20μg/ml
PI
Annexin V
Apoptosis %
ns
Alamandine μg/ml
Sham
VEGF(10ng/ml)
VEGF(10ng/ml)+Alamandine(5μg/ml)
VEGF(10ng/ml)+Alamandine(10μg/ml)
VEGF(10ng/ml)+Alamandine(20μg/ml)
b
cell index
hours
c
cell index
hours
d
0hour
24hour
Sham
VEGF
VEGF+5
VEGF+10
VEGF+20
Alamandine μg/ml
e
4hour
8hour
Wound recovery at 24 hours (%)
Average tube numbers
f
VEGF
VEGF+5
VEGF+10
Alamandine μg/ml
Sprout density (norm. to VEGF)

Unedited

a, flow cytometric analysis of apoptosis in HRMECs treated with different concentrations (5, 10, 20μg/ml) of Alamandine (left) and its corresponding quantitative analysis (right). b-c, The results of RTCA migration (b) and proliferation (c) assays performed to determine the effects of different concentrations (5, 10, 20μg/ml) of Alamandine on VEGF-induced proliferation and migration of HRMECs. d-f, The results of wound healing assay (d), tube-formation assay (e), and aortic rings assay (f), which were performed to examine the role of Alamandine in VEGF-induced angiogenesis in HRMECs. VEGF: 10ng/ml. All the results are expressed as mean ± SEM (n=5 per group; NS indicates not significant, *P<0.05, **P<0.01, ***P<0.001, ****P<0.0001, compared with VEGF group; #P < 0.001, compared with Sham group).

Fig. 5 Effects of Alamandine on hypoxia-induced HIF-1α/VEGF pathway activation and apoptosis in HRMECs.

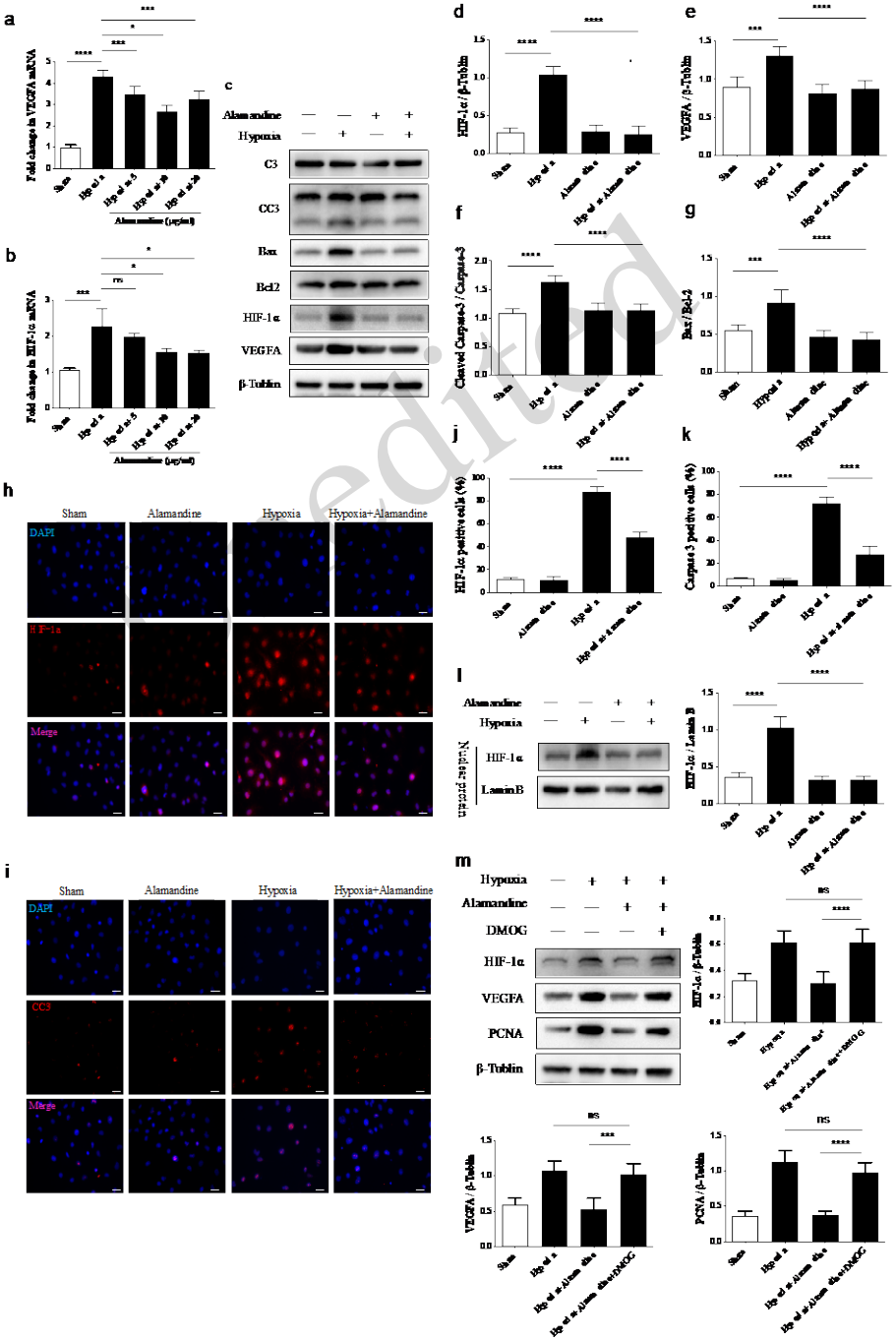

a-b, The mRNA expression levels of VEGF (a) and HIF-1α (b) in HRMECs from different groups determined by RT-PCR method.

c, The protein expression levels of C3, CC3, Bax, Bcl2, HIF-1α, VEGF, and β-Actin determined by Western blot in HRMECs from Sham, Alamandine, Hypoxia, and Hypoxia+Alamandine groups. d-g, The corresponding densitometric analysis of HIF-1α (d), VEGF (e), CC3/C3 (f), and Bax/Bcl2 (g) protein expression. β-Actin was detected as the loading control. h-i, Representative immunofluorescence images of HRMECs labeled with HIF-1α (h) and CC3 (i) from Sham, Alamandine, Hypoxia, and Hypoxia+Alamandine groups (HIF-1α, red; CC3, red; DAPI, blue. scale bars, 100μm). j-k, The corresponding quantification of HIF-1α- positive (j) or CC3-positive (k) cells in chosen images. l, The nuclear protein expression levels of HIF-1α and Lamin B determined by Western blot in HRMECs from Sham, Alamandine, Hypoxia, and Hypoxia+Alamandine groups (left) and its corresponding densitometric analysis (right). m, The protein expression levels of HIF-1α, VEGF, and PCNA determined by Western blot in HRMECs from Sham, Hypoxia, Hypoxia+Alamandine, and Hypoxia+Alamandine+DMOG groups, and the corresponding densitometric analysis. All the results are expressed as mean ± SEM (n=5 per group; NS indicates not significant, *P<0.05, **P<0.01, ***P<0.001, ****P<0.0001).

Fig. 6 Effects of Alamandine on pathological neovascularization in the retinas of OIR mice.

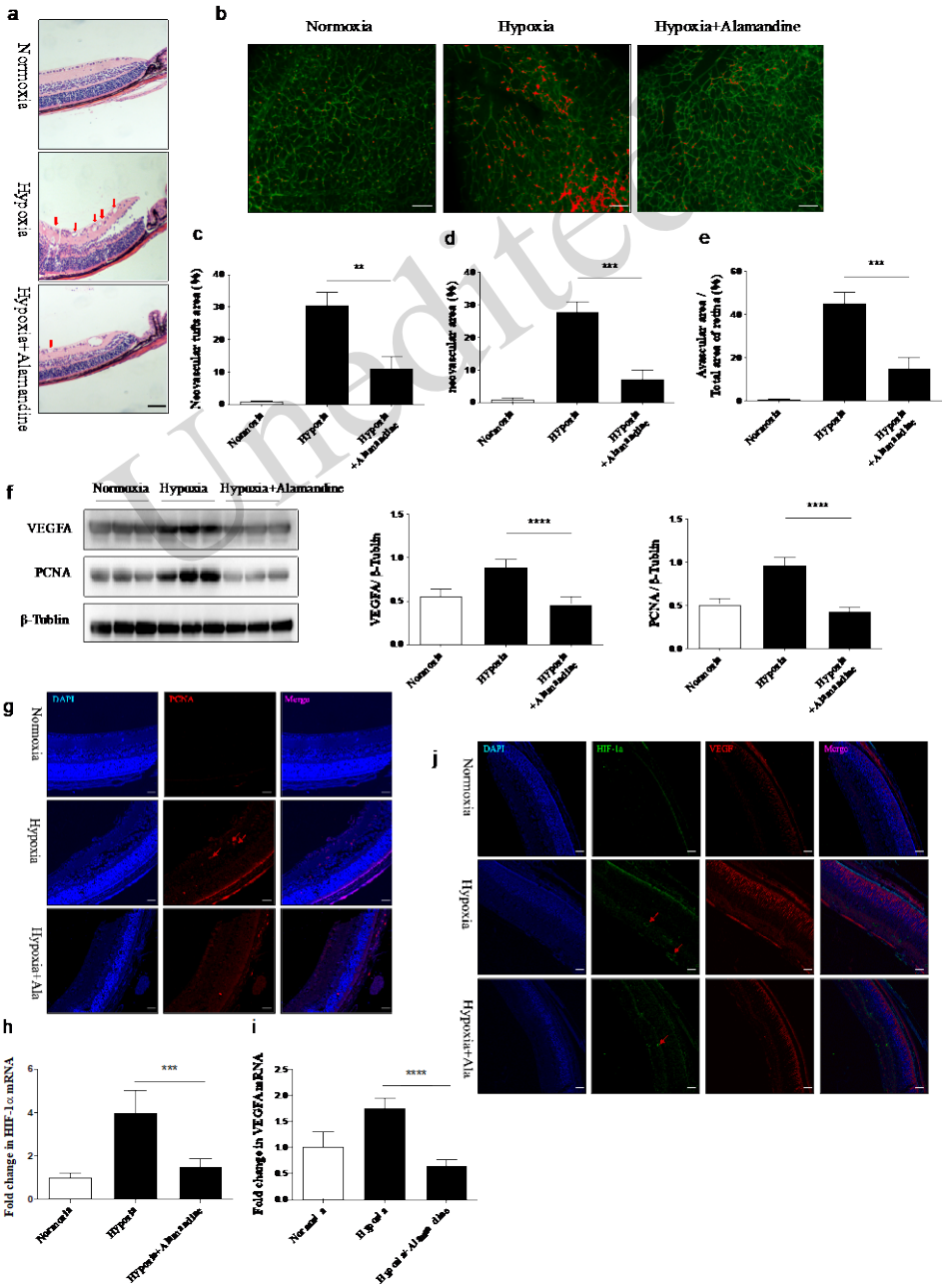

Mouse retinas were harvested from the normoxia group, hypoxia group, and hypoxia+Alamandine group. a, Representative

images of staining retinal paraffin sections with hematoxylin-eosin (HE) from the given groups (scale bars, 200μm). b, Representative images of retinal whole-mount immunostaining with IB4 (scale bars, 100μm) from the given groups (blood vessels, green; neovascularized areas, red). c-e, The corresponding quantification of avascular areas / total areas (c), neovascular tufts areas (d), and avascular areas (e). f, The protein expression levels of VEGF, PCNA, and β-Actin determined by Western blot in retinal tissues from the given groups (left) and its corresponding densitometric analysis (right). β-Actin was detected as the loading control. g, Representative immunofluorescence images of retinal paraffin sections stained with PCNA and DAPI from the given groups (PCNA, red; DAPI, blue). h-i, The mRNA expression levels of HIF-1α (h) and VEGF (i) in retinal tissues from the given groups determined by RT-PCR method. All mRNA expression was normalized to β-Actin. j, Representative immunofluorescence images of retinal paraffin sections stained with HIF-1α, VEGF, and DAPI from the given groups (HIF-1α, red; VEGF, red; DAPI, blue). All the results are expressed as mean ± SEM (n=6 per group; NS indicates not significant, *P<0.05, **P<0.01, ***P<0.001, ****P<0.0001).

Fig. 7 Effects of Alamandine on glial cells dysfunction and inflammation in the retinas of OIR mice.

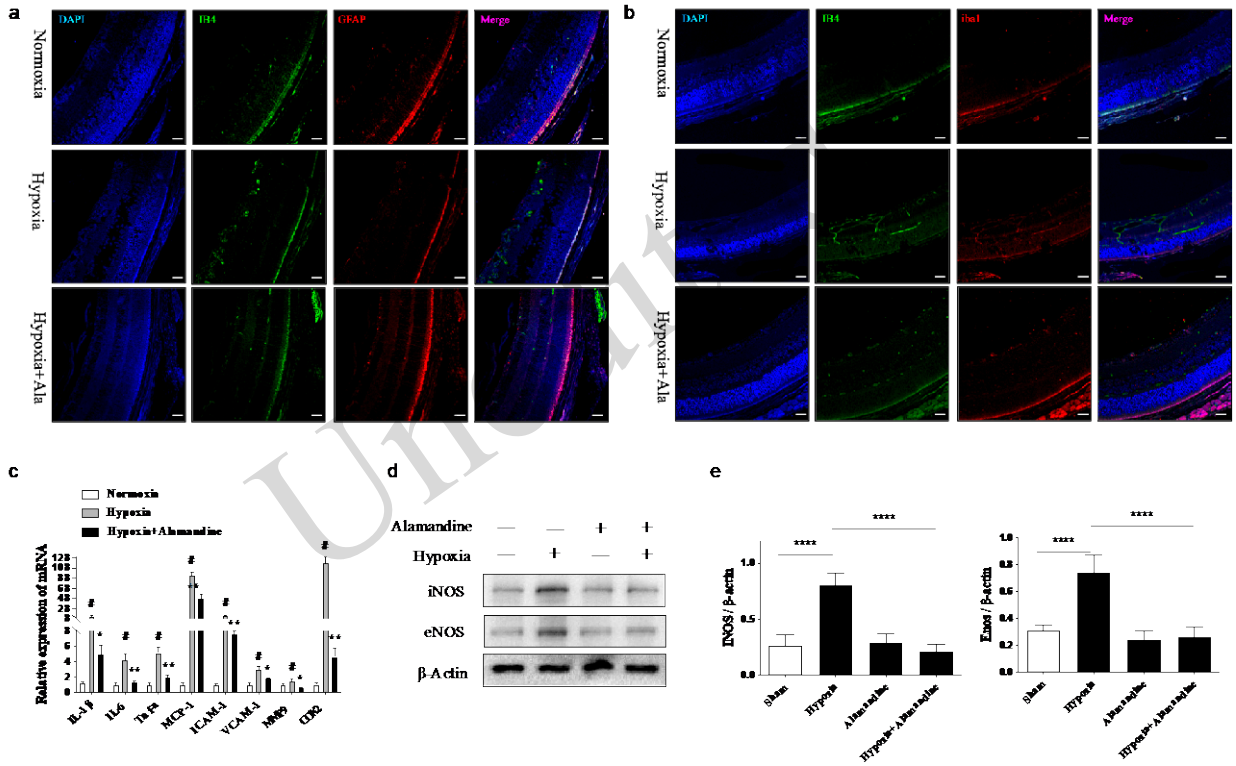

Mouse retinas were harvested from the normoxia group, hypoxia group, and hypoxia+Alamandine group. a, Representative immunofluorescence images of retinal paraffin sections stained with IB4, GFAP, and DAPI from the given groups (IB4, green; GFAP, red; DAPI, blue). b, Representative immunofluorescence images of retinal paraffin sections stained with IB4, Iba1, and DAPI from the given groups (IB4, green; iba1, red; DAPI, blue). c, The mRNA expression levels of IL-1β, IL-6, TNF-α, MCP-1, MMP-9, and COX-2, as well as ICAM-1 and VCAM-1 in retinal tissues from the given groups determined by RT-PCR method. All mRNA expression was normalized to β-Actin. d, The protein expression levels of INOS, ENOS, and β-Actin were determined by Western blot in retinal tissues from the given groups. e, The corresponding densitometric analysis of iNOS and eNOS protein expression. β-Actin was detected as the loading control. All the results are expressed as mean ± SEM (n=5 per group; NS indicates not significant, *P<0.05, **P<0.01, ***P<0.001, ****P<0.0001).

Fig. 8 Role of MrgD in the protective effects of Alamandine against hypoxia-induced pathological angiogenesis in mice.

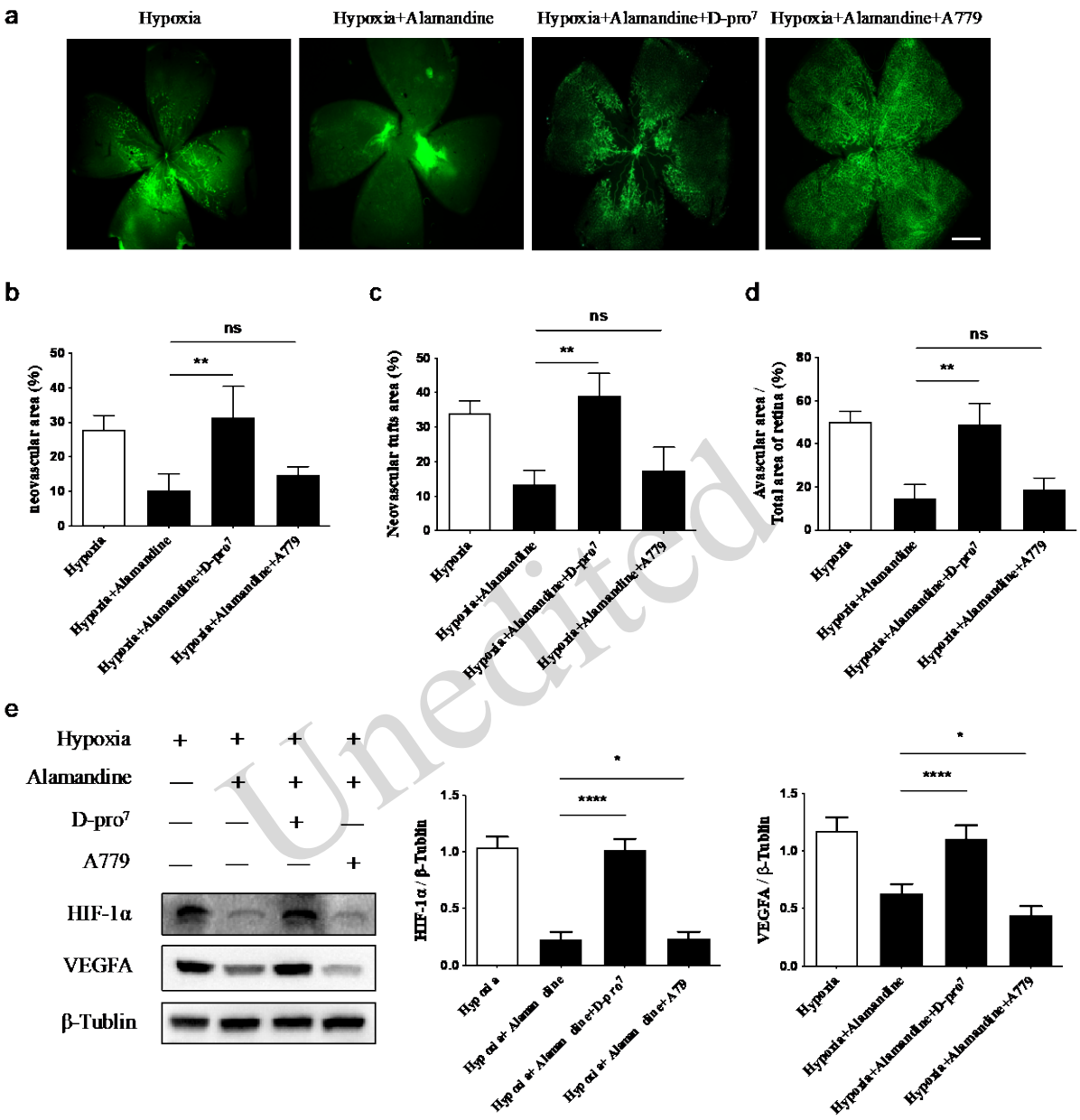

a, Representative images of retinal whole-mount immunostaining with IB4 from the different groups (scale bars, 500μm). b-d, The corresponding quantification of avascular areas / total areas (b), neovascular tufts areas (c), and avascular areas (d). e, The protein expression levels of HIF-1α, VEGF, and β-Actin determined by Western blot in mice retinas from the different groups (left) and the corresponding densitometric analysis (right). β-Actin was detected as the loading control. All the results are expressed as mean ± SEM (n=6 per group; NS indicates not significant, *P<0.05, **P<0.01, ***P<0.001, ****P<0.0001).

References

Ahmed NEMB, Murakami M, Kaneko S, et al., 2016. The effects of hypoxia on the stemness properties of human dental pulp stem cells (DPSCs). *Sci Rep*, 6:35476. https://doi.org/10.1038/srep35476

Amraei R, Rahimi N, 2020. Covid-19, renin-angiotensin system and endothelial dysfunction. *Cells*, 9(7):1652. https://doi.org/10.3390/cells9071652

Aouiss A, Anka Idrissi D, Kabine M, et al., 2019. Update of inflammatory proliferative retinopathy: ischemia, hypoxia and

Unedited

angiogenesis. *Curr Res Transl Med*, 67(2):62-71.
https://doi.org/10.1016/j.retram.2019.01.005

Au NPB, Ma CHE, 2022. Neuroinflammation, microglia and implications for retinal ganglion cell survival and axon regeneration in traumatic optic neuropathy. *Front Immunol*, 13:860070.
https://doi.org/10.3389/fimmu.2022.860070

Boddu SHS, Acharya D, Hala V, et al., 2023. An update on strategies to deliver protein and peptide drugs to the eye. *ACS Omega*, 8(39):35470-35498.
https://doi.org/10.1021/acsomega.3c02897

Brenner M, Messing A, 2021. Regulation of gfap expression. *ASN Neuro*, 13:1759091420981206.
https://doi.org/10.1177/1759091420981206

Broxterman EC, Hug DA, 2016. Retinopathy of prematurity: a review of current screening guidelines and treatment options. *Mo Med*, 113(3):187-190.

Chang E, Josan AS, Purohit R, et al., 2022. A network meta-analysis of retreatment rates following bevacizumab, ranibizumab, aflibercept, and laser for retinopathy of prematurity. *Ophthalmology*, 129(12):1389-1401.
https://doi.org/10.1016/j.ophtha.2022.06.042

Chang RL, Lin JW, Kuo WW, et al., 2016. Angiotensin-(1-7) attenuated long-term hypoxia-stimulated cardiomyocyte apoptosis by inhibiting HIF-1α nuclear translocation via Mas receptor regulation. *Growth Factors*, 34(1-2):11-18.
https://doi.org/10.3109/08977194.2016.1155150

Checchin D, Sennlaub F, Levavasseur E, et al., 2006. Potential role of microglia in retinal blood vessel formation. *Invest Ophthalmol Vis Sci*, 47(8):3595-3602.
https://doi.org/10.1167/iovs.05-1522

Cheng Y, Zhang M, Xu R, et al., 2024. P53 accelerates endothelial cell senescence in diabetic retinopathy by enhancing foxo3a ubiquitylation and degradation via ube2l6. *Exp Gerontol*, 188:112391.
https://doi.org/10.1016/j.exger.2024.112391

Cheng Y, Zhang M, Li CG, et al., 2025. Endothelial aggf1 promotes retinal angiogenesis by coordinating tnfsf12/fn14 signalling. *Nat Commun*, 16(1):1332.
https://doi.org/10.1038/s41467-025-55970-3

Choręziak-Michalak A, Szpecht D, Chmielarz-Czarnocińska A, et al., 2023. Comprehensive analysis of the role of gene variants in matrix metalloproteinases and their tissue inhibitors in retinopathy of prematurity: a study in the polish population. *Int J Mol Sci*, 24(20):15309.
https://doi.org/10.3390/ijms242015309

Connor KM, Krah NM, Dennison RJ, et al., 2009. Quantification of oxygen-induced retinopathy in the mouse: a model of vessel loss, vessel regrowth and pathological angiogenesis. *Nat Protoc*, 4(11):1565-1573.
https://doi.org/10.1038/nprot.2009.187

Dammann O, Hartnett ME, Stahl A, 2023. Retinopathy of prematurity. *Dev Med Child Neurol*, 65(5):625-631.
https://doi.org/10.1111/dmcn.15468

Daruich A, Bremond-Gignac D, Behar-Cohen F, et al., 2020. Retinopathy of prematurity: from prevention to treatment. *Med Sci (Paris)*, 36(10):900-907.
https://doi.org/10.1051/medsci/2020163

de Carvalho Santuchi M, Dutra MF, Vago JP, et al., 2019. Angiotensin-(1-7) and alamandine promote anti-inflammatory response in macrophages *in vitro* and *in vivo*. *Mediators Inflamm*, 2019:2401081.
https://doi.org/10.1155/2019/2401081

de Jesus ICG, Scalzo S, Alves F, et al., 2018. Alamandine acts via mrgd to induce ampk/no activation against Ang II hypertrophy in cardiomyocytes. *Am J Physiol Cell Physiol*, 314(6):C702-C711.
https://doi.org/10.1152/ajpcell.00153.2017

de Jesus ICG, Mesquita T, Souza Santos RA, et al., 2023. An overview of alamadine/MrgD signaling and its role in cardiomyocytes. *Am J Physiol Cell Physiol*, 324(3): C606-C613.
https://doi.org/10.1152/ajpcell.00399.2021

Domińska K, Okła P, Kowalska K, et al., 2018. Angiotensin 1-7 modulates molecular and cellular processes central to the pathogenesis of prostate cancer. *Sci Rep*, 8(1):15772.
https://doi.org/10.1038/s41598-018-34049-8

Dong LJ, Li WB, Lin TT, et al., 2021. PSF functions as a repressor of hypoxia-induced angiogenesis by promoting mitochondrial function. *Cell Commun Signal*, 19(1):14.
https://doi.org/10.1186/s12964-020-00684-w

Duan YQ, Beli E, Li Calzi S, et al., 2018. Loss of angiotensin-converting enzyme 2 exacerbates diabetic retinopathy by promoting bone marrow dysfunction. *Stem Cells*, 36(9):1430-1440.
https://doi.org/10.1002/stem.2848

Fevereiro-Martins M, Marques-Neves C, Guimarães H, et al., 2023. Retinopathy of prematurity: a review of pathophysiology and signaling pathways. *Surv Ophthalmol*, 68(2):175-210.
https://doi.org/10.1016/j.survophthal.2022.11.007

Guo Y, Gu RP, Gan DK, et al., 2020. Mitochondrial DNA drives noncanonical inflammation activation via cGAS-STING signaling pathway in retinal microvascular endothelial cells. *Cell Commun Signal*, 18(1):172.

Unedited

https://doi.org/10.1186/s12964-020-00637-3
Hartnett ME, 2023. Pathophysiology of retinopathy of prematurity. *Annu Rev Vis Sci*, 9:39-70.
https://doi.org/10.1146/annurev-vision-093022-021420
He XM, Wen SY, Tang XX, et al., 2024. Glucagon-like peptide-1 receptor agonists rescued diabetic vascular endothelial damage through suppression of aberrant sting signaling. *Acta Pharm Sin B*, 14(6):2613-2630.
https://doi.org/10.1016/j.apsb.2024.03.011
Hu ZZ, Mao XY, Chen MK, et al., 2022. Single-cell transcriptomics reveals novel role of microglia in fibrovascular membrane of proliferative diabetic retinopathy. *Diabetes*, 71(4):762-773.
https://doi.org/10.2337/db21-0551
Huang H, 2020. Pericyte-endothelial interactions in the retinal microvasculature. *Int J Mol Sci*, 21(19).
https://doi.org/10.3390/ijms21197413
Karlstetter M, Scholz R, Rutar M, et al., 2015. Retinal microglia: just bystander or target for therapy? *Prog Retin Eye Res*, 45:30-57.
https://doi.org/10.1016/j.preteyeres.2014.11.004
Lashkari K, Hirose T, Yazdany J, et al., 2000. Vascular endothelial growth factor and hepatocyte growth factor levels are differentially elevated in patients with advanced retinopathy of prematurity. *Am J Pathol*, 156(4):1337-1344.
https://doi.org/10.1016/s0002-9440(10)65004-3
Lautner RQ, Villela DC, Fraga-Silva RA, et al., 2013. Discovery and characterization of alamandine: a novel component of the renin-angiotensin system. *Circ Res*, 112(8):1104-1111.
https://doi.org/10.1161/circresaha.113.301077
Li HG, Horke S, Förstermann U, 2014. Vascular oxidative stress, nitric oxide and atherosclerosis. *Atherosclerosis*, 237(1):208-219.
https://doi.org/10.1016/j.atherosclerosis.2014.09.001
Li N, Gao S, Wang J, et al., 2019. Anti-apoptotic effect of interleukin-17 in a mouse model of oxygen-induced retinopathy. *Exp Eye Res*, 187:107743.
https://doi.org/10.1016/j.exer.2019.107743
Li P, Chen XR, Xu F, et al., 2018. Alamandine attenuates sepsis-associated cardiac dysfunction via inhibiting MAPKs signaling pathways. *Life Sci*, 206:106-116.
https://doi.org/10.1016/j.lfs.2018.04.010
Mintz-Hittner HA, Kennedy KA, Chuang AZ, 2011. Efficacy of intravitreal bevacizumab for stage 3+ retinopathy of prematurity. *N Engl J Med*, 364(7):603-615.
https://doi.org/10.1056/NEJMoa1007374
Moravski CJ, Skinner SL, Stubbs AJ, et al., 2003. The renin-angiotensin system influences ocular endothelial cell proliferation in diabetes: Transgenic and interventional studies. *Am J Pathol*, 162(1):151-160.
https://doi.org/10.1016/s0002-9440(10)63806-0
Nicosia RF, Ottinetti A, 1990. Growth of microvessels in serum-free matrix culture of rat aorta. A quantitative assay of angiogenesis in vitro. *Lab Invest*, 63(1):115-122.
Park BM, Phuong HTA, Yu LM, et al., 2018. Alamandine protects the heart against reperfusion injury via the MrgD receptor. *Circ J*, 82(10):2584-2593.
https://doi.org/10.1253/circj.CJ-17-1381
Paul M, Poyan Mehr A, Kreutz R, 2006. Physiology of local renin-angiotensin systems. *Physiol Rev*, 86(3):747-803.
https://doi.org/10.1152/physrev.00036.2005
Perelli RM, O'sullivan ML, Zarnick S, et al., 2021. Environmental oxygen regulates astrocyte proliferation to guide angiogenesis during retinal development. *Development*, 148(9):dev199418.
https://doi.org/10.1242/dev.199418
Phipps JA, Dixon MA, Jobling AI, et al., 2019. The renin-angiotensin system and the retinal neurovascular unit: a role in vascular regulation and disease. *Exp Eye Res*, 187:107753.
https://doi.org/10.1016/j.exer.2019.107753
Rathi S, Jalali S, Patnaik S, et al., 2017. Abnormal complement activation and inflammation in the pathogenesis of retinopathy of prematurity. *Front Immunol*, 8:1868.
https://doi.org/10.3389/fimmu.2017.01868
Rattner A, Williams J, Nathans J, 2019. Roles of HIFs and VEGF in angiogenesis in the retina and brain. *J Clin Invest*, 129(9):3807-3820.
https://doi.org/10.1172/jci126655
Rivera JC, Madaan A, Zhou TE, et al., 2016. Review of the mechanisms and therapeutic avenues for retinal and choroidal vascular dysfunctions in retinopathy of prematurity. *Acta Paediatr*, 105(12):1421-1433.
https://doi.org/10.1111/apa.13586
Sabri K, Ells AL, Lee EY, et al., 2022. Retinopathy of prematurity: a global perspective and recent developments. *Pediatrics*, 150(3):e2021053924.
https://doi.org/10.1542/peds.2021-053924
Santiago AR, Madeira MH, Boia R, et al., 2020. Keep an eye on adenosine: its role in retinal inflammation. *Pharmacol Ther*, 210:107513.

Unedited

https://doi.org/10.1016/j.pharmthera.2020.107513
Schleifenbaum J, 2019. Alamandine and its receptor MrgD pair up to join the protective arm of the renin-angiotensin system. *Front Med (Lausanne)*, 6:107.
https://doi.org/10.3389/fmed.2019.00107
Song MA, Dasgupta C, Zhang LB, 2015. Chronic losartan treatment up-regulates AT_1R and increases the heart vulnerability to acute onset of ischemia and reperfusion injury in male rats. *PLoS ONE*, 10(7):e0132712.
https://doi.org/10.1371/journal.pone.0132712
Tual-Chalot S, Allinson KR, Fruttiger M, et al., 2013. Whole mount immunofluorescent staining of the neonatal mouse retina to investigate angiogenesis *in vivo*. *J Vis Exp*, (77):e50546.
https://doi.org/10.3791/50546
Uemura A, Fruttiger M, D'Amore PA, et al., 2021. VEGFR1 signaling in retinal angiogenesis and microinflammation. *Prog Retin Eye Res*, 84:100954.
https://doi.org/10.1016/j.preteyeres.2021.100954
Vallée A, Guillevin R, Vallée JN, 2018. Vasculogenesis and angiogenesis initiation under normoxic conditions through Wnt/β-catenin pathway in gliomas. *Rev Neurosci*, 29(1):71-91.
https://doi.org/10.1515/revneuro-2017-0032
Voigt AP, Mullin NK, Stone EM, et al., 2021. Single-cell RNA sequencing in vision research: insights into human retinal health and disease. *Prog Retin Eye Res*, 83:100934.
https://doi.org/10.1016/j.preteyeres.2020.100934
Wang YH, Fang JW, Niu T, et al., 2023. Serum Ang-1/Ang-2 ratio may be a promising biomarker for evaluating severity of diabetic retinopathy. *Graefes Arch Clin Exp Ophthalmol*, 261(1):49-55.
https://doi.org/10.1007/s00417-022-05745-z
Xu Y, Lu X, Hu YG, et al., 2018. Melatonin attenuated retinal neovascularization and neuroglial dysfunction by inhibition of HIF-1α-VEGF pathway in oxygen-induced retinopathy mice. *J Pineal Res*, 64(4):e12473.
https://doi.org/10.1111/jpi.12473
Yang CX, Wu XG, Shen YH, et al., 2020. Alamandine attenuates angiotensin II-induced vascular fibrosis via inhibiting p38 MAPK pathway. *Eur J Pharmacol*, 883:173384.
https://doi.org/10.1016/j.ejphar.2020.173384
Yang XF, Wang JP, Chen C, 2021. Serum VEGF and Ang-2 levels in infants before and after laser treatment for retinopathy of prematurity. *Fetal Pediatr Pathol*, 40(5):407-413.
https://doi.org/10.1080/15513815.2020.1721625
Zhang XZ, Zhang F, Xu X, 2024. Single-cell RNA sequencing in exploring the pathogenesis of diabetic retinopathy. *Clin Transl Med*, 14(7):e1751.
https://doi.org/10.1002/ctm2.1751
Zhao K, Xu TH, Mao YK, et al., 2022a. Alamandine alleviated heart failure and fibrosis in myocardial infarction mice. *Biol Direct*, 17(1):25.
https://doi.org/10.1186/s13062-022-00338-6
Zhao K, Jiang YP, Zhang J, et al., 2022b. Celastrol inhibits pathologic neovascularization in oxygen-induced retinopathy by targeting the miR-17-5p/HIF-1α/VEGF pathway. *Cell Cycle*, 21(19):2091-2108.
https://doi.org/10.1080/15384101.2022.2087277
Zhao K, Hua DX, Yang CX, et al., 2023. Nuclear import of Mas-related G protein-coupled receptor member D induces pathological cardiac remodeling. *Cell Commun Signal*, 21(1):181.
https://doi.org/10.1186/s12964-023-01168-3
Zhu P, Verma A, Prasad T, et al., 2020. Expression and function of Mas-related G protein-coupled receptor D and its ligand Alamandine in retina. *Mol Neurobiol*, 57(1):513-527.
https://doi.org/10.1007/s12035-019-01716-4
Zimna A, Kurpisz M, 2015. Hypoxia-inducible factor-1 in physiological and pathophysiological angiogenesis: applications and therapies. *Biomed Res Int*, 2015:549412.
https://doi.org/10.1155/2015/549412

Unedited

Supplementary information:

Figs. S1-S5

Fig. S1: ACE, AGT, and AT2 mRNA expression levels were lower in hypoxia-induced HRMECs versus control.

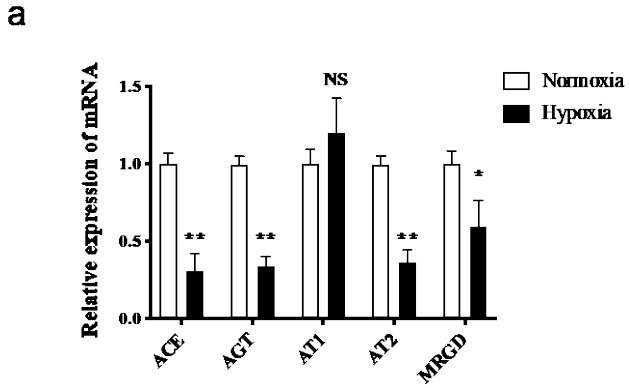

a, The mRNA expression levels of ACE, AGT, AT1, AT2, and MrgD in HRMECs from different groups determined by RT-PCR method. All mRNA expression was normalized to β-Actin. All the results are expressed as mean ± SEM (n=6 per group; NS indicates not significant, *P<0.05, **P<0.01, ***P<0.001, compared with normoxia group).

Fig. S2: Alamandine ameliorated Ang II-induced EC apoptosis, migration, and proliferation.

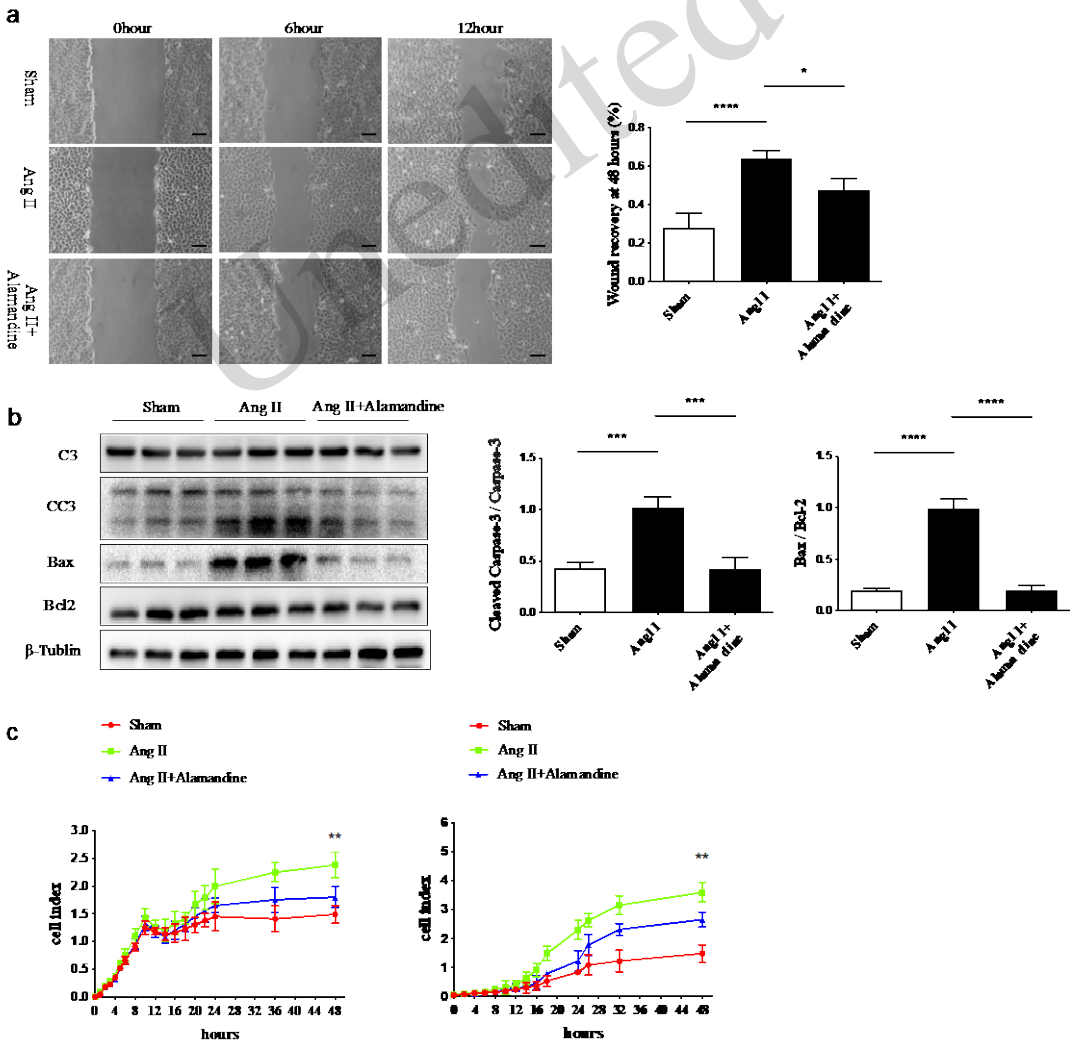

a, The wound healing assay was performed to examine the role of Alamandine in Ang II-induced angiogenesis in HRMECs. b, The protein expression levels of C3, CC3, Bax, Bcl2, and β-Tublin in HRMECs from different groups determined by Western blot (left) and the corresponding densitometric analysis (right). β-Tublin was detected as the loading control. c, The results of RTCA

Unedited

migration and proliferation assays performed to determine the effects of Alamandine on Ang II-induced proliferation and migration of HRMECs. All the results are expressed as mean ± SEM (n=5 per group; NS indicates not significant, *P<0.05, **P<0.01, ***P<0.001, ****P<0.0001, compared with VEGF group; #P < 0.001, compared with Sham group).

Fig. S3: Alamandine alone has no significant adverse effects on retinal vessel development in a normal retina.

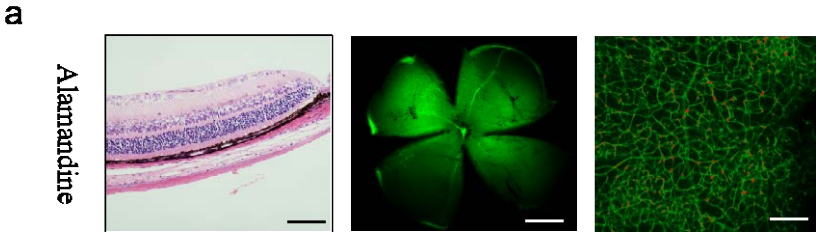

a, Representative images of staining retinal paraffin sections with hematoxylin-eosin (HE) (left; scale bars, 200μm), and retinal whole-mount immunostaining with IB4 (middle: scale bars, 500μm; right: scale bars, 100μm) from the given group (blood vessels, green; neovascularized areas, red).

Fig. S4. Role of MrgD in the protective effects of Alamandine against VEGF-induced angiogenesis in HRMECs.

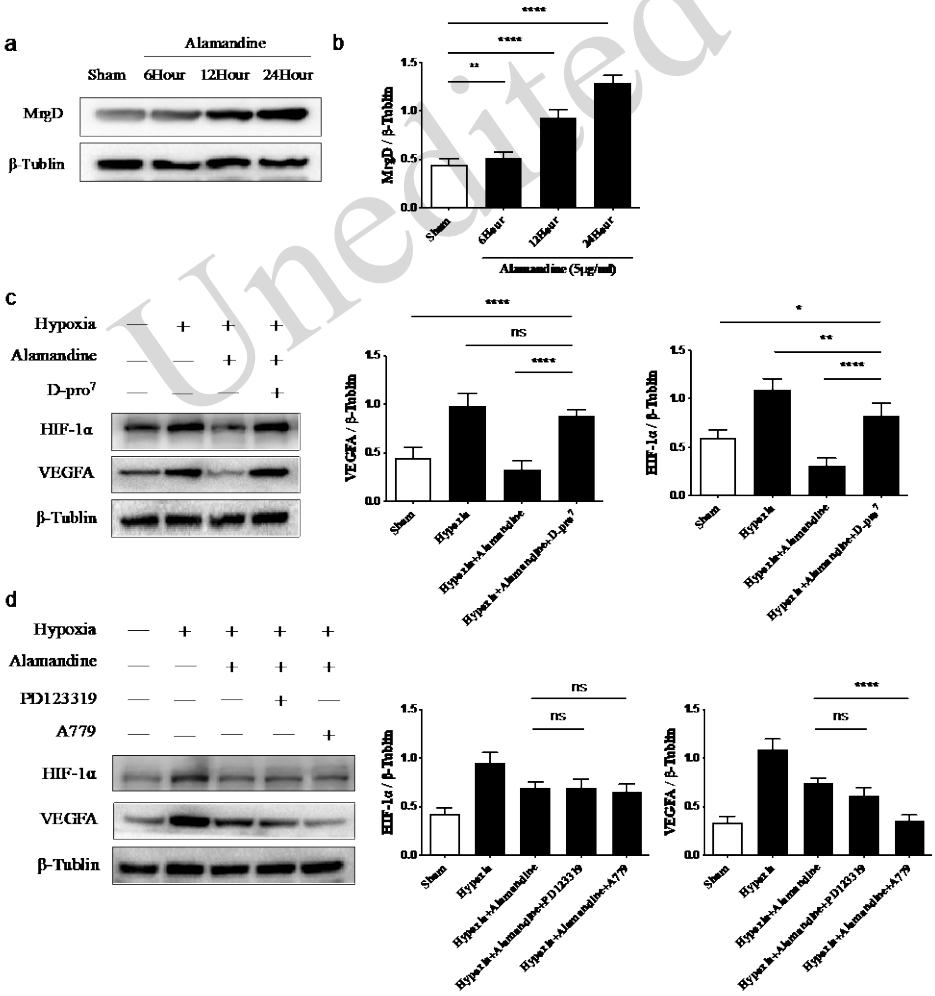

Unedited

a-b, The protein expression levels of MrgD, and β-Actin determined by Western blot in HRMECs treated with different inductive times of Alamandine (10μg/ml) (a), and the corresponding densitometric analysis (b). c-d, The protein expression levels of HIF-1α, VEGF, and β-Actin determined by Western blot in HRMECs from the different groups (left) and the corresponding densitometric

analysis (right). β-Actin was detected as the loading control. All the results are expressed as mean ± SEM (n=5 per group; NS indicates not significant, *P<0.05, **P<0.01, ***P<0.001, ****P<0.0001).

Fig. S5: Role of MrgD in the protective effects of Alamandine against glial cell dysfunction and inflammation in the retinas of OIR mice.

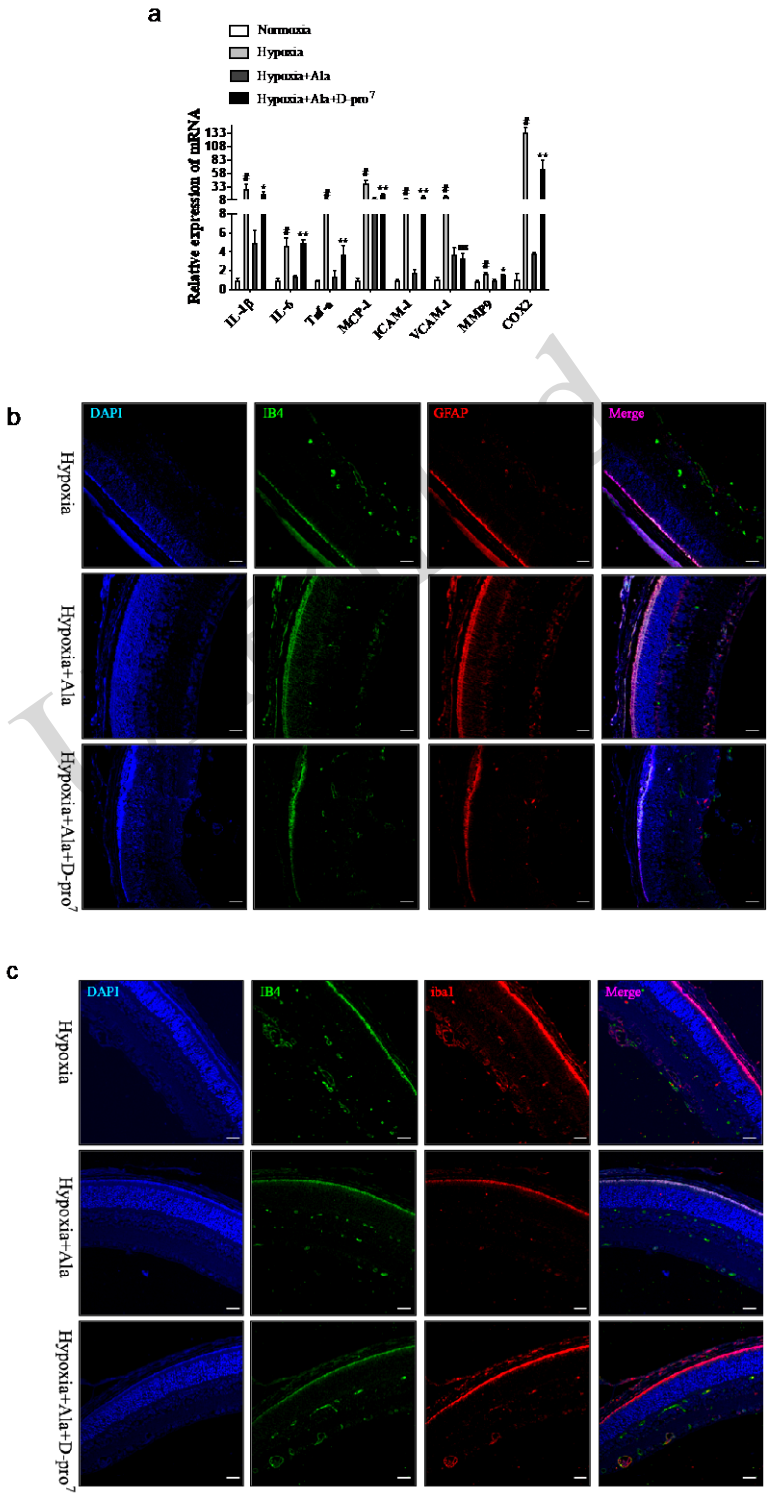

Mouse retinas were harvested from the hypoxia group, hypoxia+Alamandine group, and hypoxia+Alamandine+D-Pro^7 group. a, The mRNA expression levels of IL-1β, IL-6, TNF-α, MCP-1, MMP-9, and COX-2, as well as ICAM-1 and VCAM-1 in retinal

tissues from the given groups determined by RT-PCR method. All mRNA expression was normalized to β-Actin. b, Representative immunofluorescence images of retinal paraffin sections stained with IB4, GFAP, and DAPI from the given groups (IB4, green; GFAP, red; DAPI, blue). c, Representative immunofluorescence images of retinal paraffin sections stained with IB4, Iba1, and DAPI from the given groups (IB4, green; iba1, red; DAPI, blue). All the results are expressed as mean ± SEM (n=5 per group; NS indicates not significant, *P<0.05, **P<0.01, ***P<0.001, ****P<0.0001).

Unedited